Technical University of Munich

Department of Informatics

Bachelor's Thesis in Informatics

Wavefront Coding Techniques for Extended Depth of Field in Light Field Microscopy

By

Felix Wechsler

Technical University of Munich

Department of Informatics

Bachelor's Thesis in Informatics

Wavefront Coding Techniques for Extended Depth of Field in Light Field Microscopy

Wellenfront Kodierung für erweiterte Tiefenschärfe in Lichtfeld Mikroskopie

Author: Felix Wechsler

Supervisor: PD Dr. rer. nat. habil. Tobias Lasser

Advisors: M. Sc. Anca-Elena Stefanoiu

M. Sc. Josué Page Vizcaíno

Submission date: October 10, 2018

I confirm that this bachelor's thesis is my own work and I have documented all sources and material used.

Garching, 10.10.2018 Felix Wechsler

Abstract

Light field microscopy is a scanless technique for high speed 3D imaging of fluorescent specimens. A conventional microscope can be turned into a light field microscope by placing a microlens array in front of the camera, allowing a full spatio-angular capture of the light field in a single snapshot. The recorded information can be used to volumetrically reconstruct the imaged sample. In this thesis we focus on the point spread function of the whole system and derive it using Fourier optics. To increase the resolution further we apply wavefront coding via cubic phase masks and compare the resolution between the different setups.

Contents

Abstract iv

1 Introduction to Light Field Microscopy 1

1.1 History of Light Field . . . 1
1.2 Foundations of Light Field Microscopy . . . 2

2 Optical Model 4

2.1 Scalar Diffraction Theory . . . 5
2.2 Lens as Phase Transformer . . . 6
2.3 Fourier Property of a Lens . . . 8
2.4 Phase Mask . . . 11

3 Light Field Microscope 13

3.1 Lens Setup . . . 13
3.2 4f-system . . . 13
3.3 Microlens Array . . . 16
3.4 Debye Integral . . . 16
3.5 Full Fresnel Propagation for First Lens . . . 17

4 Implementation 18

4.1 Fast Fourier Transform . . . 18
4.2 Lens Propagation . . . 20
4.3 Code for 4f-system . . . 20
4.4 Code for MLA with PM . . . 22
4.5 Sampling . . . 23

5 Simulation Results 25

5.1 Point Spread Function . . . 25
5.2 Reconstruction Results . . . 34

6 Conclusion 37

1 Introduction to Light Field Microscopy

1.1 History of Light Field

Microscopy was originally a method to magnify small specimens which are in the size of milli- or micrometers. Due to its construction and working principle it was only possible to get a 2D slice of the 3D object. However, biological processes do not elapse in the 2D space but more in the volume of the system. This drawback of conventional microscopy was the starting point of developing techniques to get 3D information of the system.
In this bachelor's thesis we will focus on the light field microscope (LFM) which was proposed by the Stanford Computer Graphics Laboratory [Lev+06] under the lead of Marc Levoy who was a pioneer in light field science.
Actually the term light field is quite old and is highly connected with integral photography invented by Gabriel Lippmann in the early 20th century. In [AW92] light field is defined by a 5D function which means that for every point in space we have got a radiance in a specific direction. The space has got 3 degrees of freedom and the direction is fully determined by two angles (see Figure 1.1b). Therefore, the radiance is a scalar function $F(x, y, z, \varphi, \theta)$. Starting with

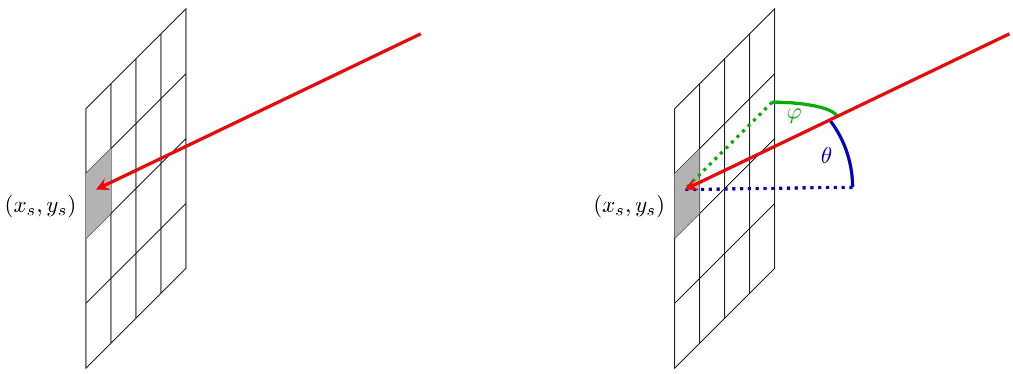

(a) Sensor with position detection (b) Sensor with position and angle detection

Figure 1.1: Camera sensor

that definition it is possible to imagine a camera which is able to capture such light fields (see Figure 1.1). Instead of only spatial information we furthermore obtain angular information about

the scene we are photographing. This extra information allows us to do some 3D reconstruction [LH96]. Unfortunately a standard sensor is not sensitive to the direction but in [Ng+05] such a camera was first designed. There they place a microlens array (MLA) in front of the sensor. This MLA adds the extra angular information to the image in cost of spatial information. This method is always a tradeoff between spatial and angular resolution. Using conventional ray optics the group was able to take photos with their camera which can be refocused after the photo was taken. Today the plenoptic camera 1.0 [Ng+05], the plenoptic camera 2.0 [GLC11] are commonly used but also more advanced setups with a MLA where not all of the lenslets have the same focal length [Chr12] exist. In 2012 consumer hand-held cameras were sold by Lytro which ceased it's operations in 2018. Today Raytrix [1] is the leading company in light field technology.
The technique was already adapted for microscopy by [Lev+06] in 2006. Again the MLA is the key element for the light field capturing. The optical model is similar to that of plenoptic cameras and despite diffraction the results were good. The next step was done by the Stanford Computer Graphics Laboratory introducing computational intensive wave optics to model the diffraction [Bro+13]. Wave optics increased the resolution dramatically but still lacked in non uniform resolution and artifacts at the native focus plane. Around 2014, in his PhD thesis ([Coh+15] and [Coh+14]) Cohen successfully tackled the non uniform resolution and the artifacts with a phase mask (PM) placed at multiple positions in the system. Since then no significant steps were done in the LFM topic regarding resolution or new setups.

1.2 Foundations of Light Field Microscopy

The basis of the current state-of-the-art LFM is given in [Bro+13] where a wave optics approach was used. The previous ray optics mathematics was not usable anymore and completely new methods were derived. It all starts by the assumption that our specimen emits spherical waves and the volume does not scatter the light. This is only valid if our object mainly consists out of water or other materials that permit light to pass through. The origin of the waves is fluorescence. The light is then is filtered by a 535 nm filter in front of the optical setup. Since the fluorescent points emit waves randomly and independently of all other points the waves only interfere with themselves. This means that the final image is a sum over point source waves gone through the system. In [Bro+13] the captured image is mathematically described by the integral

$$f(x,y) = \iiint |h(x,y,x_p,y_p,z_p)|^2 \, g(x_p,y_p,z_p) \, \mathrm{d}x_p \, \mathrm{d}y_p \, \mathrm{d}z_p \tag{1.1}$$

[1] www.raytrix.de

where x, y are the position on the sensor plane. The integration is done over the observed volume and g is the intensity function. h is called the point spread function (PSF) of the system and will be derived in Chapter 3. The discrete version of the above equation is given by

$$\mathbf{f} = H\mathbf{g} \tag{1.2}$$

where vector $\mathbf{f}$ is the final light field, vector $\mathbf{g}$ is the discrete volume being reconstructed and H the matrix describing the imaging process. The explanation for the reconstruction of the image can be found in the paper [Bro+13]. The PSF of the LFM will be the main topic of this thesis and will be derived from scratch throughout this work.

2 Optical Model

In this chapter we will explain our optical model describing the LFM. Optics can be done either in ray or wave optics. Ray optics is mainly the technique for setups without diffraction. Wave optics is the general approach to describe any optical system. However in practice it is complicated to calculate larger systems with wave optics. Since we are interested in the diffraction effects we choose wave optics as our main tool. Furthermore the PM cannot be modeled by ray optics because the phase of a ray does not exist in ray optics.
In the beginning we shortly want to explain the basis of wave optics. A full and broad introduction to wave optics can be found in [Goo96]. Here we present only the necessary parts to understand the system of our microscope. Wave optics is especially important to describe effects which occur due to diffraction. Sommerfeld defined diffraction in [Som54] as "any deviation of light rays from rectilinear paths which cannot be interpreted as reflection or refraction".
One main principle of wave optics is the idea that every point on a wavefront is the origin of another wave. All these new wavelets together generate a new wavefront. This idea is visualized

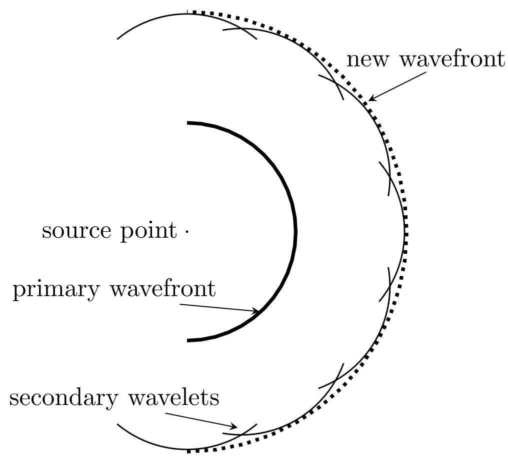

Figure 2.1: Huygens-Fresnel principle

in Figure 2.1 and was first proposed by Huygens [Huy90]. Later Fresnel [Fre19] used this property together with interference to get a mathematical formalism for diffraction patterns.
In wave optics we describe light by electromagnetic waves which propagate through space. A

wave with its origin at point P is described by

$$U(x, y, z) = \frac{A}{r} \exp(ikr) \tag{2.1}$$

where r is the distance between point P and (x, y, z) and A some amplitude. k is the so called wave number of the wave and is defined by $k = \frac{2\pi n}{\lambda}$ where λ is the wavelength of light and n is the refraction index of the medium. In literature the propagation is sometimes denoted by an opposite sign in the exponent. This is important because some of our references use the opposite convention.

2.1 Scalar Diffraction Theory

Light is an electromagnetic field which has components in all three directions. However in most cases it is enough to solve diffraction problems with a scalar approach. In general diffraction integrals quantify the situation when an electromagnetic wave hits an aperture and we want to know the electric field behind the aperture. All these equations can be derived out of Maxwell's

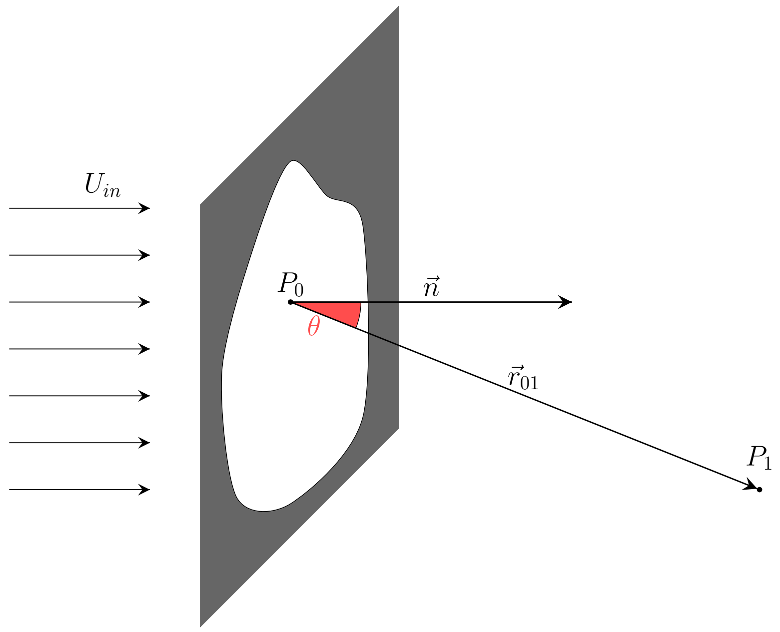

Figure 2.2: Diffraction of an aperture

equations and a full treatise can be found in [Goo96] or [Gu00].
Depending on which boundary conditions are chosen three different solutions exist which are named Rayleigh-Sommerfeld I, II and Kirchhoff integral. In [WM64] it was shown that for an aperture much larger than the wavelength and for moderate angles all theories are identical.

For simplicity we choose Rayleigh-Sommerfeld I:

$$U(P_1) = \frac{1}{i\lambda} \iint_\Sigma U(P_0) \frac{\exp(ikr_{01})}{r_{01}} \cos(\theta)\, \mathrm{d}s \tag{2.2}$$

θ is the angle between the normal vector of the aperture and the vector $\vec{r}_{01}$. The cos-obliquity factor is sometimes set to 1. Σ is the aperture which is hit by the wave. The scenario is drawn in Figure 2.2. Later we'll use the integral in rectangular coordinates:

$$U(x, y, z) = \frac{z}{i\lambda} \iint_\Sigma U(\xi, \eta) \frac{\exp(ikr)}{r^2}\, \mathrm{d}\xi \mathrm{d}\eta \tag{2.3}$$

where $r = \sqrt{z^2 + (\xi - x)^2 + (\eta - y)^2}$.

Fresnel Diffraction

To get an analytical expression of more complex situations we do some approximations on Equation 2.3. We want to use first order Taylor series to approximate the square root. It is valid to write $\sqrt{a+b} \approx a(1 + \frac{b}{2a})$ if $b \ll a$. In our case we can use this relation by requiring $z^2 \gg x^2 + y^2$. Using this condition we also can substitute r in the denominator by z. All together this simplifies the integral to:

$$U(x, y, z) = \frac{\exp(ikz)}{i\lambda} \int_{-\infty}^{\infty} \int_{-\infty}^{\infty} P(\xi, \eta) U(\xi, \eta) \frac{\exp\left(\frac{ik}{2z}\left((x - \xi)^2 + (y - \eta)^2\right)\right)}{z}\, \mathrm{d}\xi \mathrm{d}\eta \tag{2.4}$$

The aperture Σ will be a circular one in our case. This turns the integral to one over a pupil function $P(\xi, \eta)$.

Limits of Fresnel Diffraction

To get accurate results we have to ensure that our angles inside the optical path are rather small. According [Smi+93] up to a numerical aperture of NA=0.5 these requirements are fulfilled. Above that we must use scalar Debye theory which does not make the assumption of small angles. One could also use the general vectorial diffraction theory which models effects of polarization.

2.2 Lens as Phase Transformer

In wave optics we need a different description of a lens because the standard rules do not apply anymore. As previously shown a wave has an amplitude and a phase. Here we assume an

ideal, thin lens which does not reflect any intensity. The wave number depends on the medium the wave is propagating through. In air the wave number is given by $k = \frac{2\pi}{\lambda}$ and in another medium by $k_n = n \cdot k$ where n is the refraction index. For a lens made of glass n is around 1.5. Due to this different wave number there will be a optical path difference between light passing through glass and light passing through air. Neglecting reflected intensity (Fresnel equations describe intensity change) only the phase ϕ of the wave changes. This change is described by the transmission function $t_l(x, y)$ which we want to derive. Simply said a lens is nothing else than a phase transformer.
We furthermore assume that incoming and emerging points of the wave through the lens are identical. This assumption is valid if we use a thin lens and paraxial rays.
A wave travelling distance d in air has the phase shift $\phi = d \cdot k$. To get the phase of the wave travelling through the lens in Figure 2.3b we add the different stages of travelling through air and the lens together to

$$\phi = k\,(d - b - \Delta_1 - \Delta_2) + k\,n\,(\Delta_1 + \Delta_2 + b) \tag{2.5}$$

where Δ_2 is the small part drawn in Figure 2.3c, Δ_1 is the part of the left part of the lens respectively. Using Pythogoras' theorem we obtain

$$\Delta_{1/2} = R_{1/2} - l_{1/2} = R_{1/2} - \sqrt{R_{1/2}^2 - h^2} = R_{1/2} - \sqrt{R_{1/2}^2 - (x^2 + y^2)} \tag{2.6}$$

where x, y are the positions on which the wave impacts the lens. $h^2 = x^2 + y^2$ is given by the front view in Figure 2.3a. Finally the phase shift due to the lens is:

$$\begin{aligned}\phi = k\,(n-1)\,&\left(R_1 - \sqrt{R_1^2 + (x^2 + y^2)}\right)\\ &+ k\,(n-1)\,\left(R_2 - \sqrt{R_2^2 + (x^2 + y^2)}\right)\\ &+ k\,(n-1)\,b + kd\end{aligned} \tag{2.7}$$

A global phase for a wave can usually be omitted. Therefore the last term can be removed. Again we approximately express the square root via the first order of the series $\sqrt{R_1^2 + (x^2 + y^2)} \approx R_1 \left(1 + \frac{x^2+y^2}{2R_1^2}\right)$. This simplifies the term to:

$$\phi = -k\,(n-1)\,\frac{x^2 + y^2}{2}\left(\frac{1}{R_1} + \frac{1}{R_2}\right) \tag{2.8}$$

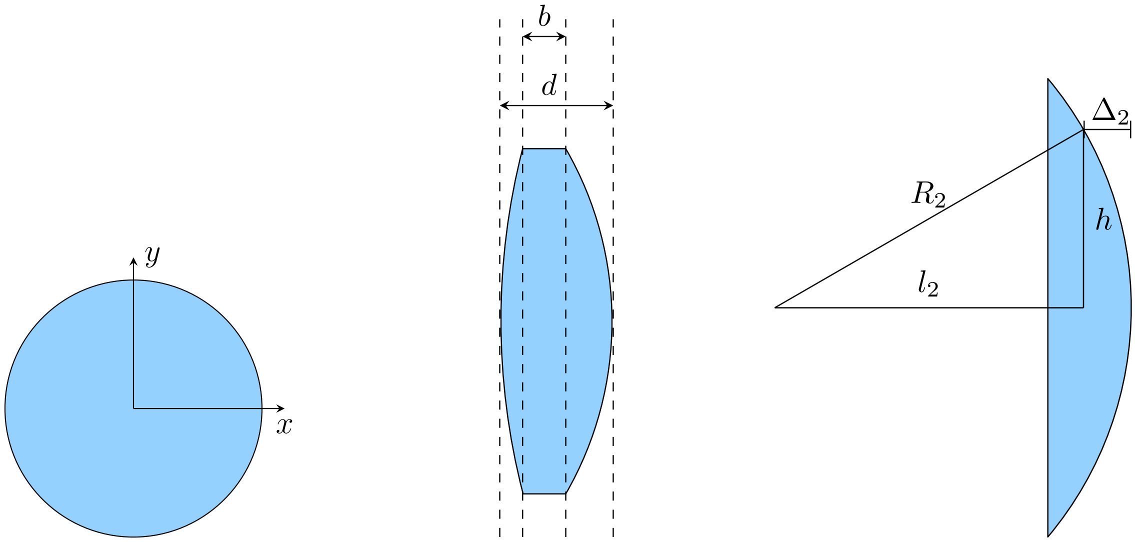

(a) front view lens (b) side view lens (c) right part of lens

Figure 2.3: Ideal thin lens

Now we can insert Lensmaker's equation which defines the focal length of a lens:

$$\frac{1}{f} = (n-1)\left(\frac{1}{R_1} + \frac{1}{R_2}\right) \tag{2.9}$$

This finally gives the complex transmittance

$$t_l(x,y) = \exp\left(-i\,\frac{k}{2f}\,(x^2+y^2)\right). \tag{2.10}$$

This expression was derived for a double-convex lens but according to [Goo96] it is also true for other types of lenses like double-concave.

2.3 Fourier Property of a Lens

First we will derive the property of a conventional objective with air as the surrounding medium and afterwards modify the equation to describe the situation with water in front of the lens because in [Bro+13] a water dipping objective is used in practice.

Surrounding medium air

In the previous parts we introduced the transmittance function of a lens and the Fresnel diffraction. Based on these concepts we can derive the Fourier property of a thin lens. This property is especially important to allow fast numerical calculations of optical systems.

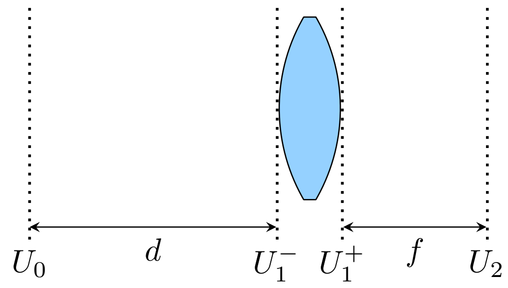

Figure 2.4: Thin lens

Figure 2.4 shows the situation we want to model. Having a field U_0 at position d in front of the lens, we want to calculate the electrical field U_2 exactly one focal length f behind the lens. The first step is to propagate the field until the lens using Fresnel approximation. This is valid for rather small angles which we will assume now. We use Equation 2.4:

$$U_1^-(x,y) = \frac{\exp(ikd)}{i\lambda} \int_{-\infty}^{\infty}\int_{-\infty}^{\infty} P(\xi,\eta) U_0(\xi,\eta) \frac{\exp\left(\frac{ik}{2d}((x-\xi)^2 + (y-\eta)^2)\right)}{d} \mathrm{d}\xi \mathrm{d}\eta \tag{2.11}$$

The wave transmission through the lens is given by Equation 2.10. If we plug in Equation 2.11 into the lens transmission given by Equation 2.10 we get the field after the lens. We furthermore assume that the lens is quite large and we can leave out the pupil function $P(x,y)$.

$$U_1^+(x,y) = \exp\left(-i\frac{k}{2f}(x^2+y^2)\right) \frac{\exp(ikd)}{i\lambda} \tag{2.12}$$

$$\int_{-\infty}^{\infty}\int_{-\infty}^{\infty} P(\xi,\eta) U_0(\xi,\eta) \frac{\exp\left(\frac{ik}{2d}((x-\xi)^2 + (y-\eta)^2)\right)}{d} \mathrm{d}\xi \mathrm{d}\eta \tag{2.13}$$

From U_1^- we do another Fresnel propagation with Equation 2.4 until the back focal plane of the objective:

$$U_2(x,y) = \frac{\exp(ikf)}{i\lambda} \iint_{-\infty}^{\infty} U_1^+(\nu,\tau) \frac{\exp\left(\frac{ik}{2f}\left((x-\nu)^2 + (y-\tau)^2\right)\right)}{f} \mathrm{d}\nu \mathrm{d}\tau \tag{2.14}$$

When plugging U_1^+ in, the quadratic term of the lens cancels out. Note that the exponential prefactor has now a positive sign:

$$\begin{aligned} U_2(x,y) = &\exp\left(i\frac{k}{2f}(x^2+y^2)\right)\frac{\exp(ik(d+f))}{i\lambda i\lambda}\iiiint_{-\infty}^{\infty} \\ &U_0(\xi,\eta)\frac{\exp\left(\frac{ik}{2d}((\nu-\xi)^2+(\tau-\eta)^2)\right)}{d}\frac{\exp\left(-\frac{ik}{f}(\nu x+\tau y)\right)}{f}\,\mathrm{d}\xi\mathrm{d}\eta\mathrm{d}\nu\mathrm{d}\tau \end{aligned} \tag{2.15}$$

Now we want to evaluate the integral over ν and τ. The relevant part of Equation 2.15 is:

$$\iint_{-\infty}^{\infty}\exp\left(i\frac{k}{2d}((\nu-\xi)^2+(\tau-\eta)^2\right)\exp\left(-i\frac{k}{f}(\nu x+\tau y)\right)\mathrm{d}\nu\mathrm{d}\tau \tag{2.16}$$

A substitution with $\nu' = \nu-\xi$ and $\tau' = \tau-\eta$ gives us:

$$\iint_{-\infty}^{\infty}\exp\left(i\frac{k}{2d}(\nu'^2+\tau'^2\right)\exp\left(-i\frac{k}{f}(\nu' x+\tau' y)\right)\exp\left(-i\frac{k}{f}(\xi x+\eta y)\right)\mathrm{d}\nu'\mathrm{d}\tau' \tag{2.17}$$

The first part is a scaled Fourier transform of a Gaussian. One can look that up that in analysis books:

$$\iint_{-\infty}^{\infty}\exp\left(\frac{ic}{2}(t_1^2+t_2^2)\right)\exp\left(-i(t_1\omega_1+t_2\omega_2)\right)\mathrm{d}t_1\mathrm{d}t_2 = \frac{2\pi i}{c}\exp\left(-\frac{i}{2c}(\omega_1^2+\omega_2^2)\right) \tag{2.18}$$

Using Equation 2.18 we can reduce Equation 2.17 to:

$$\frac{2\pi i d}{k}\exp\left(-\frac{ikd}{2f^2}(x^2+y^2)\right)\exp\left(-i\frac{k}{f}(\xi x+\eta y)\right) \tag{2.19}$$

Finally we can plug Equation 2.19 into Equation 2.15 and use $k=\frac{2\pi}{\lambda}$:

$$\begin{aligned} U_2(x,y) = &\frac{\exp\left(i\frac{k}{2f}\left(1-\frac{d}{f}\right)(x^2+y^2)\right)\exp(ik(d+f)}{i\lambda f}\iint_{-\infty}^{\infty} \\ &U_0(\xi,\eta)\exp\left(-i\frac{k}{f}(\xi x+\eta y)\right)\mathrm{d}\xi\mathrm{d}\eta \end{aligned} \tag{2.20}$$

We can also leave out constant phase factors like $\frac{1}{i}$ and $\exp(ik(d+f))$.

$$U_2(x,y) = \frac{\exp\left(i\frac{k}{2f}\left(1-\frac{d}{f}\right)(x^2+y^2)\right)}{\lambda f}\iint_{-\infty}^{\infty}U_0(\xi,\eta)\exp\left(-i\frac{k}{f}(\xi x+\eta y)\right)\mathrm{d}\xi\mathrm{d}\eta \tag{2.21}$$

The result is in accordance with a different derivation in [Goo96] and is quite interesting because it says that the Fourier transform of the input field U_0 is the output field U_2 times a phase factor. However if one chooses $d = f$ Equation 2.21 reduces further to an exact (scaled) Fourier transform:

$$U_2(x,y) = \frac{1}{\lambda f} \iint_{-\infty}^{\infty} U_0(\xi,\eta) \exp\left(-i\frac{k}{f}(\xi x + \eta y)\right) \mathrm{d}\xi \mathrm{d}\eta = \frac{2\pi}{\lambda f}\, \mathcal{F}(U_0) \left(\frac{k}{f}x, \frac{k}{f}y\right) \tag{2.22}$$

Equation 2.22 is often called Fourier property of a lens since the output field at the back focal plane is the Fourier transform of the input field at the front focal plane.

Water in front of the lens

In microscopy it is quite common to have a water-dipping objective leading to a higher numerical aperture which results in a increased resolution. In this situation everything before the lens has the different wave number $k_n = n_w \cdot k$ where n_w is the refraction index of water. It is easy to see that Equation 2.21 changes a little bit to:

$$U_2(x,y) = \frac{\exp\left(i\frac{k}{2f}\left(1 - \frac{d}{n \cdot f}\right)(x^2+y^2)\right)}{\lambda f} \iint_{-\infty}^{\infty} U_0(\xi,\eta) \exp\left(-i\frac{k}{f}(\xi x + \eta y)\right) \mathrm{d}\xi \mathrm{d}\eta \tag{2.23}$$

In conclusion we note that having water in front of the lens does not change the Fourier transform behaviour of the lens. It causes a scaling of the distance d by the factor $1/n$.

2.4 Phase Mask

A PM or phase-shift mask is a optical element that changes the phase of a wave. The most popular specific PM is a lens since the transition results in a quadratic phase shift specified in Equation 2.10. In general the transmission function of a PM is:

$$t_{\mathrm{PM}}(x,y) = \exp\left(i\phi_{\mathrm{PM}}(x,y)\right) \tag{2.24}$$

However in practice not all functions are feasible especially when using a passive optical element. In [Coh+15] they were using a cubic PM for most of the simulations:

$$t_{\mathrm{PM}}(x,y) = \exp\left(i\alpha(x^3+y^3)\right) \tag{2.25}$$

Such a cubic PM can be manufactured if one simply cuts a cubic surface into a transparent plastic piece. The parameter α is then determined by thickness and refraction index of the material. In Figure 2.5 the surface of a cubic phase mask is drawn.

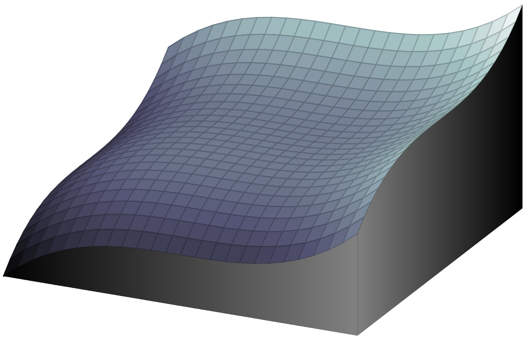

Figure 2.5: surface of cubic PM

It is also possible to change the phase of waves via active optical components called spatial light modulators (SLM). Such devices have a specific amount of pixels on which they can separately change the phase of the wave hitting that part of the SLM. In [Coh+15] non-trivial PM functions were derived which could be implemented using a SLM.

3 Light Field Microscope

In this chapter we want to use the previously derived optical methods to model our LFM. This chapter is mainly based on [Bro+13], [Coh+14] and [Coh+15].

3.1 Lens Setup

The schematic setup of the LFM is drawn in Figure 3.1. In the experiments from [Coh+15] this setup looks different but is optically equivalent to the one shown here.
Starting with the 4f-system we proceed modelling the microlens array and finish the chapter with a full mathematical description of our microscope.

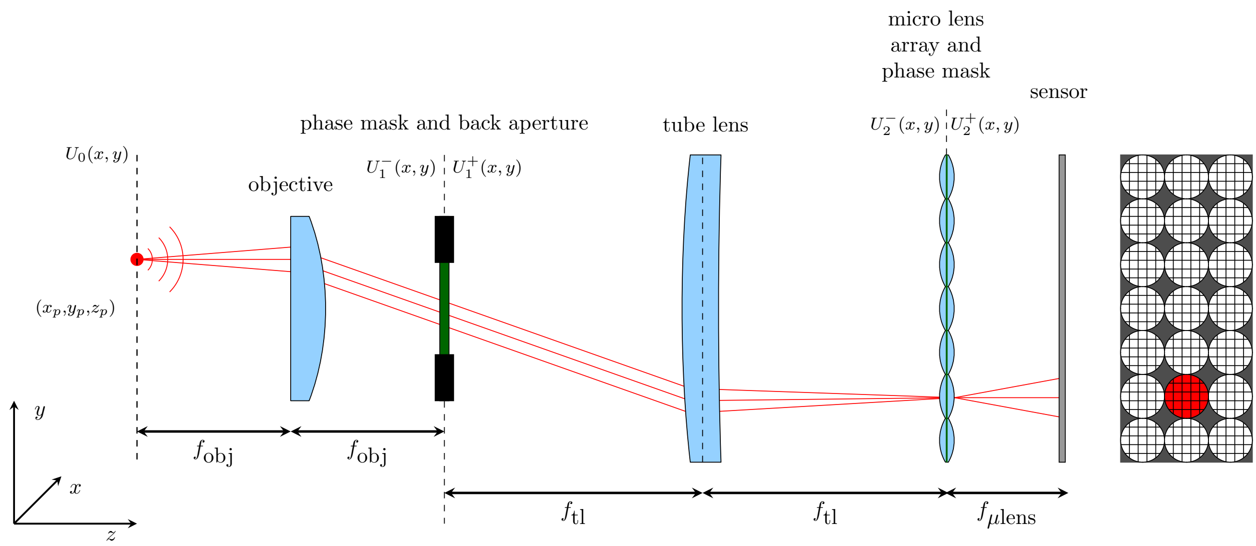

Figure 3.1: Setup of the LFM

3.2 4f-system

The first part of our microscope consists of a 4f-system. This part is separately sketched in Figure 3.2. To obtain a real image of an object placed at the front focal plane of the objective

U_0 the screen has to be placed at the back focal plane of the tube lens. This setup does not fulfill the lens equation and is described by Abbe imaging theory [Gu00]. In our LMF we assume

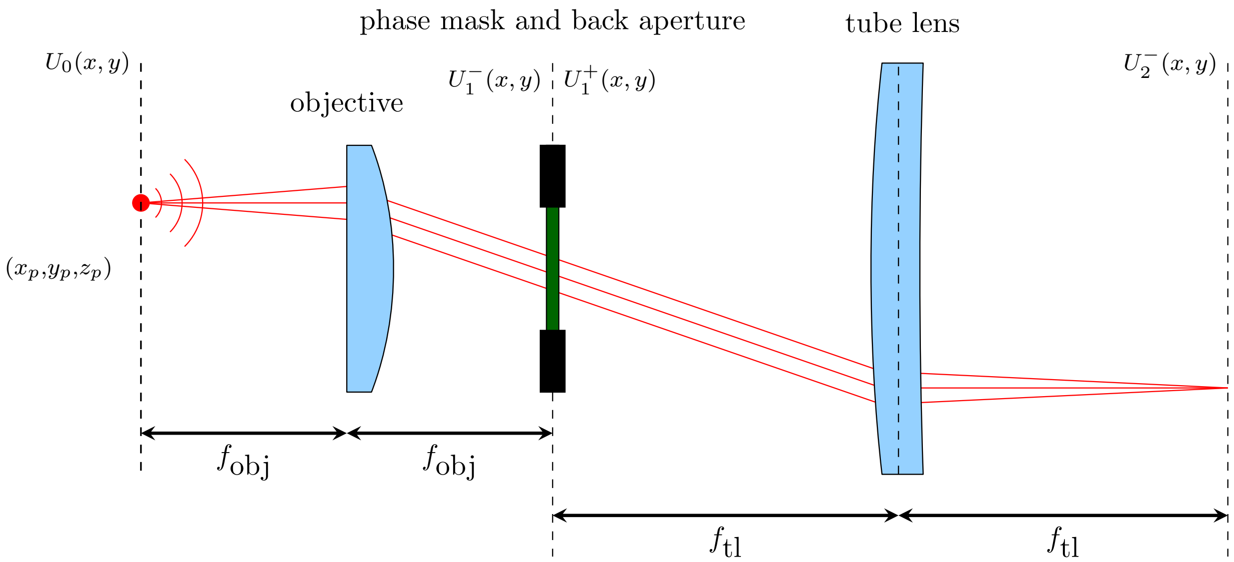

Figure 3.2: 4f-system

that we have got many point source emitters somewhere in the object. This assumption is valid since we observe a fluorescent specimen which emits waves randomly. We furthermore assume that none of the waves interfere with each other because fluorescent objects emit incoherent light. The only interference of the wave is with itself which makes it possible to treat every single point source independently of the others.

Our first optical model is the one from [Coh+15]. Starting with a point source at position (x_p, y_p, z_p) we can propagate the wave until the front focal plane U_0 using Equation 2.1.

$$U_0(x,y) = \frac{A \exp\left(ikr \operatorname{sign}(-z_p)\right)}{r} \tag{3.1}$$

where $r = \sqrt{(x-x_p)^2 + (y-y_p)^2 + z_p}$ and the signum function is necessary because if z_p is positive the source would be in front of U_0 and therefore we would propagate it back to U_0 (actually the signum function is not needed for perfect spherical waves and lenses but with aberrations it would have an effect.). In the previous chapter we derived that the electrical field at the back focal plane of the objective U_1^- is the Fourier transform of the front focal plane U_0. So we obtain with Equation 2.22:

$$U_1^-(x,y) = \frac{1}{\lambda f_{\text{obj}}} \iint_{-\infty}^{\infty} U_0(\xi,\eta) \exp\left(-i\frac{k}{f_{obj}}(\xi x + \eta y)\right) \mathrm{d}\xi \mathrm{d}\eta \tag{3.2}$$

U_1^- is the field in the back focal plane of the first lens which is called objective lens with focal length f_{obj}.

The plane is referred to as the Fourier plane of the 4f-system due to the Fourier transform behaviour of the first lens. In [Coh+15] the cubic PM is placed in that point. Additionally the objective used has a back aperture in the Fourier plane which acts as a low pass filter. This is reasonable because high frequencies correspond to large distances to the axis of the system and the back aperture obstructs these distances. To get U_1^+ we simply multiply U_1^- with the pupil function of the aperture and the PM:

$$U_1^+(x,y) = U_1^-(x,y) \cdot \exp\left(i\alpha(x^3+y^3)\right) \cdot P_{\text{obj}}(x,y) \tag{3.3}$$

The pupil function is defined by $P_{\text{obj}}(x,y) = H\left(1 - \frac{x^2+y^2}{d_{\text{obj}}^2/4}\right)$ (H is the Heaviside step function) and the diameter $d_{\text{obj}} = 2\text{NA}f$. NA is the numerical aperture objective and has the value 0.5. To obtain the field at the native image plane U_2^- we do another Fourier transform and get:

$$U_2^-(x,y) = \frac{1}{\lambda f_{\text{tl}}} \iint_{-\infty}^{\infty} U_1^+(\xi,\eta) \exp\left(-i\frac{k}{f_{tl}}(\xi x + \eta y)\right) \, \mathrm{d}\xi \mathrm{d}\eta \tag{3.4}$$

f_{tl} is the focal length of the tube lens. Without a microlens array this setup would return an image of a defocused point source. In ray optics this image would be an uniform disk but in wave optics we later see that the output is a defocused airy pattern which has oscillating patterns inside this disk.

Water Dipping Objective

In [Coh+15] it is mentioned that the used lens is a water immersion objective and we have got water in front of the first lens. This changes Equation 3.1 to

$$U_0(x,y) = \frac{A \exp\left(ik_n r \,\text{sign}(-z_p)\right)}{r} \tag{3.5}$$

where the wave number is $k_n = n \cdot k$ and n is the refraction index of water. The exact Fourier property is not achieved if the object is placed in front of the lens with the distance f_{obj}. Looking at Equation 2.23 we see that the distance has to be $d = n \cdot f_{\text{obj}}$. This means that the presence of water requires slight changes of the setup: The object needs to be placed in greater distance to the front of the lens.

3.3 Microlens Array

The microlens array consists of many small lenses with PMs inside the lenses. To model these PM we modify the transmission function of a single microlens.

$$t_{\mu\text{lens}}(x, y) = \exp\left(-i\frac{k}{2f_{\mu\text{lens}}}(x^2 + y^2) - i\beta(x^3 + y^3)\right) \tag{3.6}$$

β is determined by the surface and material of the PM. To model the MLA we convolve the transmission function with the Dirac comb function:

$$U_2^+(x, y) = U_2^-(x, y)\,(t_{\mu\text{lens}}(x, y) * \text{III}(x/p_{\mu\text{ml}}, y/p_{\mu\text{ml}})) \tag{3.7}$$

where $p_{\mu\text{ml}}$ is the size of one microlens. Now we obtained U_2^+, the field behind the microlens array. The last step is a Fresnel propagation from U_2^+ to the sensor placed one microlens focal length $f_{\mu\text{lens}}$ away. Again we neglect constant phase factors.

$$U_3(x, y) = \frac{1}{\lambda f_{\mu\text{lens}}} \iint_{-\infty}^{\infty} U_2^+(\xi, \eta) \exp\left(i\frac{k}{2f_{\mu\text{lens}}}\left((x - \xi)^2 + (y - \eta)^2\right)\right) \tag{3.8}$$

$U_3(x, y)$ is the full analytical expression for the electrical field of an input point source placed at (x_p, y_p, z_p).
Due to the incoherence of the fluorescent object the final PSF is given by:

$$h(x, y) = |U_3(x, y)|^2 \tag{3.9}$$

In comparison of Equation 3.8 to the final equation in [Coh+15] we only neglected constant phase factors and an obliquity factor in Equation 3.1.

3.4 Debye Integral

For the 4f-system another mathematical description is given in [Bro+13]. This model is based on the Debye theory derived in [Gu00] but is unable to include the PM. The Debye theory does not assume paraxial rays, considers aberration effects and thus is more accurate and can be used for high numerical aperture of values up to 0.7. The Debye integral is given by

$$\begin{aligned} U(u,v) = \frac{M}{f_{\mathrm{obj}}^2\lambda^2} \exp\left(-\frac{iu}{4\sin^2(\alpha/2)}\right) \\ \int_0^\alpha P(\theta)\exp\left(-\frac{iu\sin^2(\theta/2)}{2\sin^2(\alpha/2)}\right) J_0\left(\frac{\sin(\theta)}{\sin\alpha}\right)\sin\theta\mathrm{d}\theta \end{aligned} \tag{3.10}$$

where M is the magnification, $\alpha = \arcsin\left(\frac{\mathrm{NA}}{n}\right)$ the maximal half aperture angle, J_0 the zeroth order Bessel function and P the aperture of the lens including aberrations. Furthermore the coordinates are defined as

$$u = 4kz_p\sin^2(\alpha/2) \tag{3.11}$$

$$v = k\sin(\alpha)\sqrt{(x-x_p)^2+(y-y_p)^2} \tag{3.12}$$

3.5 Full Fresnel Propagation for First Lens

In Section 3.2 we did a propagation of the spherical wave until the Fourier plane and applied the Fourier property to obtain the field U_1^-. But we can also use Equation 2.23 where the point source is an arbitrary distance d in front of the lens. If the Fresnel approximation is valid both approximations are equivalent. Adapting the equation gives us:

$$U_1^-(x,y) = \frac{\exp\left(i\frac{kz_p}{2nf_{\mathrm{obj}}^2}(x^2+y^2)\right)}{\lambda f_{\mathrm{obj}}}\iint_{-\infty}^{\infty} U_0(\xi,\eta)\exp\left(-i\frac{k}{f_{\mathrm{obj}}}(\xi x+\eta y)\right)\mathrm{d}\xi\mathrm{d}\eta \tag{3.13}$$

In Chapter 5 we will compare the simulation results of Equation 3.8, Equation 3.10 and Equation 3.13.

4 Implementation

In this chapter we want to explain some details of the implementation. First we want to derive the fast numerical calculation of our integrals and after that give the concrete code for the 4f-system. We will close this chapter with some explanations of the sampling of the electrical fields.

4.1 Fast Fourier Transform

In the optics part we encountered many Fourier integrals which we have to evaluate. They have the general form:

$$F(x,y) = \iint_{-\infty}^{\infty} f(\xi,\eta)\exp\left(-2\pi i b(x\xi + y\eta)\right)\mathrm{d}\xi\mathrm{d}\eta \tag{4.1}$$

At this point we take the parameter b into the argument side $\tilde{x} = bx$ and $\tilde{y} = by$ and get the slightly different integral

$$F(\tilde{x},\tilde{y}) = \iint_{-\infty}^{\infty} f(\xi,\eta)\exp\left(-2\pi i(\tilde{x}\xi + \tilde{y}\eta)\right)\mathrm{d}\xi\mathrm{d}\eta. \tag{4.2}$$

To evaluate Fourier integrals efficiently the fast Fourier transform algorithm (FFT) was developed and in most programming languages a fast implementation is available. `MATLAB` uses `FFTW` [FJ05] and the 2D-FFT (for a vector f with length n) is defined as

$$F(k_x,k_y) = \sum_{a=1}^{n}\sum_{b=1}^{n} f(a,b)\exp\left(-2\pi i\frac{(a-1)(k_x-1)}{n}\right)\exp\left(-2\pi i\frac{(b-1)(k_y-1)}{n}\right). \tag{4.3}$$

To benefit from the FFT we have to discretize Equation 4.2 and transform it to the required form (Equation 4.3). First we evaluate the integral with the Riemann sum using N steps

$$F(\tilde{x},\tilde{y}) = \sum_{n=-N/2}^{N/2-1}\sum_{m=-N/2}^{N/2-1} f\left(\frac{Ln}{N},\frac{Lm}{N}\right)\left(\frac{L}{N}\right)^2\exp\left(-2\pi i\left(\frac{\tilde{x}Ln}{N}+\frac{\tilde{y}Lm}{N}\right)\right) \tag{4.4}$$

where we assume that $f = 0$ outside $\left[-\frac{L}{2}, \frac{L}{2}\right] \times \left[-\frac{L}{2}, \frac{L}{2}\right]$. This assumption is reasonable for most cases since we want to calculate diffraction effects which occur when light passes through specific finite slits or apertures.
Note that $\tilde{x}$ and $\tilde{y}$ are variables in the continuous frequency domain. Due to the FFT these variables are also discretized and the final resulting vector F is an array with the same size as the input array f. The input array is sampled with the distance between two points $\Delta\xi = \frac{L}{N}$ and therefore the maximum spatial frequencies are given by the Nyquist frequency

$$|f_{\max}| = \frac{1}{2\Delta\xi}. \tag{4.5}$$

Since we have got n data points we receive n frequencies by the FFT. Equally spaced this gives us

$$\left\{-\frac{1}{2\Delta\xi}, -\frac{1}{2\Delta\xi} + \frac{1}{L}, -\frac{1}{2\Delta\xi} + \frac{2}{L}, \ldots, \frac{1}{2\Delta\xi} - \frac{1}{L}\right\}. \tag{4.6}$$

$\tilde{x}$ and $\tilde{y}$ only take values out of this interval and we can express them with integers $p, q \in [-\frac{N}{2}, \frac{N}{2} - 1]$ with

$$\begin{aligned} \tilde{x} = xb = \frac{p}{L} \\ \tilde{y} = yb = \frac{q}{L} \end{aligned} \tag{4.7}$$

Inserting these expressions into Equation 4.4 results in

$$F(p,q) = \sum_{n=-N/2}^{N/2-1} \sum_{m=-N/2}^{N/2-1} f\left(\frac{Ln}{N}, \frac{Lm}{N}\right) \left(\frac{L}{N}\right)^2 \exp\left(-2\pi i \left(\frac{pn}{N} + \frac{qm}{N}\right)\right). \tag{4.8}$$

With Equation 4.7 we are able to calculate to which array index p the x position corresponds. The observation is that the input array describes an electrical field with input size L and the output array contains a field with side length $L_2 = \frac{N}{Lb}$. Later we will see that $b = \frac{1}{\lambda z}$ (z is the distance from aperture to screen) and this results in

$$L_2 = \frac{\lambda z N}{L}. \tag{4.9}$$

There is only one difference between Equation 4.4 and Equation 4.3 left due to the summation borders. The array indices p and q are currently defined from negative values to positive ones but the index from `MATLAB` is from 1 to N. The FFT definition requires the central position located at the first index of the array. Thus we have to shift the arrays to the right position which is done with *fftshift* and *ifftshift* in `MATLAB`.

More details about the FFT in `MATLAB` can be found in [Voe11].

4.2 Lens Propagation

In the previous parts we derived tools needed to calculate the propagation of light through a thin lens. In our work we used code which is similar to one of the examples in [Voe11] where the author calculates the Fraunhofer propagation of the electric field. As already shown the lens produces a Fraunhofer pattern (with some phase factors) on a screen despite the fact it was derived under Fresnel approximation. The Fraunhofer propagation is a simple Fourier transform. Requirement for this FFT propagation is an input sampling which is higher than the critical sampling otherwise the result is aliased and further propagation will create wrong patterns.
The function lensProp takes the electric field u1 at the front focal plane and the side length L1 of this field as arguments. The output is the electrical field u2 at the back focal plane. Remarkable is the scaling of the output field. The side length L2 depends on lambda, L1, z and N given by Equation 4.9.

```
function [u2,L2]=lensProp(u1,L1,lambda,z);
    [M,N] = size(u1);
    dx1 = L1/N;
    L2 = lambda*z/dx1;
    u2 = fftshift(fft2(ifftshift(u1))).*dx1.^2;
end
```

Listing 4.1: Code for field propagation through lens

This function assumes that N is odd because `MATLAB` is sensitive to the order of *ifftshift* and *fftshift* for odd and even input.

4.3 Code for 4f-system

Using the previous code we are now able to write a function which calculates the output field of an 4f-system. First we want to explain some details of our code. In our experiments we choose $\lambda = 535\,\mathrm{nm}$, $\mathrm{NA} = 0.5$, $M = 20$ and $n = 1.33$ for water.
In the first part we have got two wave numbers. One for the surrounding medium air and one for water due to the water dipping objective. Our input array has size 4095×4095. This is much larger than the real resolution of our sensor but because of the FFT we need this amount of points to fully sample the oscillations of complex and real part of the electrical field in the size of $500\,\mu\mathrm{m}$. After the 4f-system we downsample the field by bicubic interpolation to the

resolution of the sensor to prevent long reconstruction times. Note that we choose an odd side length to have a real midpoint.

```
function [psf] = calcPSFwithPhaseMask(p1, p2, p3, fobj, NA, yspace,
    xspace, lambda, M, n)
k = 2*pi/lambda; % wave number in air
kn = 2*pi/lambda*1.33; %wave number in water
fobj = fobj;
ftl = fobj*M;
A = 1; %amplitude of field
N = 4095;
mid = (N+1)/2;
Ninput = length(xspace);
LU0 = 500; %micrometer
x=linspace(-LU0/2, LU0/2, N);
y=x;
[X,Y]=meshgrid(x,y);
circ = @(x,y,r) (x.^2.+y.^2.<r.^2)*1.0;
dobj = 2*fobj*NA;
```

Listing 4.2: First part of 4f-system propagation

The next part checks if the point source is placed at the native plane which means that we have to treat it like a delta peak. The other case deals with the point source in front or behind the objective lens and we have to consider the sign of the r scalar. In fact in our setup it does not matter if the point source is a specific distance in front or behind the lens, the result is the same for both cases. But if one includes aberration effects this does not hold anymore.

```
if p3 == 0
    U0 = zeros(N,N);
    xpos = mid+round((p1/(LU0/2))*N/2);
    ypos = mid+round((p2/(LU0/2))*N/2);
    U0(xpos,ypos) = 1;
else
    r = sqrt((X-p1).^2.+(Y-p2).^2.+p3.^2);
    if p3 > 0
        r = -1*r;
    end
    U0 = -1i*A*kn/2/pi./r .* exp(1i.*kn.*r);
```

```
end
```

Listing 4.3: second part of 4f-system propagation

In the last part the effects of the lens occur. First we propagate from U_0 to the Fourier plane U_1^- and save the new output side length LU_1. Then we modify the electrical field with the cubic PM. Note that the argument of the PM is scaled to the real physical size of 20 mm and thus we divide by 10 mm. After the PM we cut a circle out of the field because the back aperture of the objective is at this position. In line 36 we do the second lens propagation with the new field dimension. Finishing the 4f-system the field has to be resized to the dimensions of the xspace arrays which is an argument of the whole function.

```
28 [U1minus, LU1] = lensProp(U0, LU0, lambda, fobj);
29 coeffU1minus = 1/lambda/fobj;
30 U1minus = coeffU1minus.*U1minus;
31
32 pmscale = LU1/LU0/(10e3);
33 pmshift = exp(1i*117*(X.^3+Y.^3).*pmscale.^3);
34 U1plus = U1minus.*pmshift.*circ(X./LU0.*LU1, Y./LU0.*LU1, dobj./2);
35
36 [U2minus, LU2] = lensProp(U1plus, LU1, lambda, ftl);
37 coeffU2minus = 1/lambda/ftl;
38 U2minus = coeffU2minus.*U2minus;
39
40 cut = round(xspace(end)/(LU2/2)*(N+1)/2);
41 psf = U2minus(mid-cut:mid+cut, mid-cut:mid+cut);
42 psf = imresize(psf,[Ninput Ninput], 'bicubic');
```

Listing 4.4: Last part of 4f-system propagation

4.4 Code for MLA with PM

The code for the PM in the MLA is straightforward. This code is already published by [Bro+13] and we only need to modify one line.

```
pmShift = -1i*5*(x1^3+x2^3)/abs(75)^3;
patternML(a,b,j) = exp(-1i*k/(2*fml(j))*xL2norm+pmShift);
```

Listing 4.5: Modification of calcML to include PM

Again the argument is normalized to the real dimension of the PM and we simply add the shift to the argument of the exp function.

4.5 Sampling

To assure that our chosen values fulfill the critical sampling we show some example pictures of the imaginary part

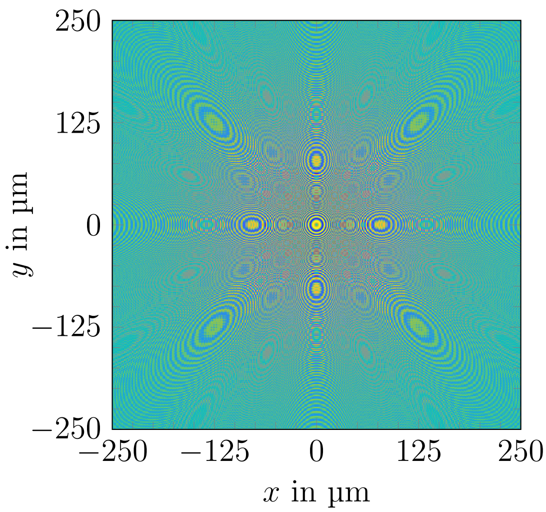

(a) Imaginary part of U_0

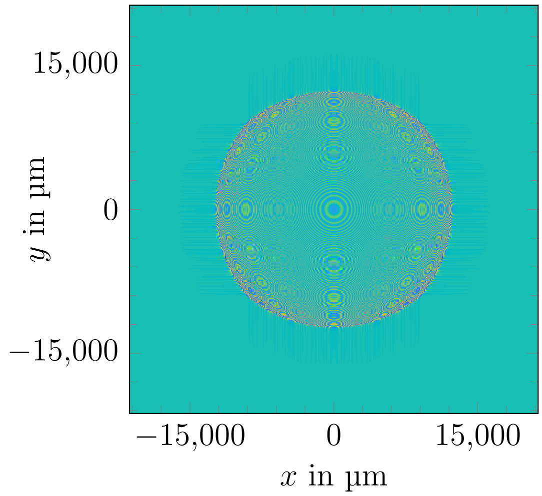

(b) Imaginary part of U_1^-

Figure 4.1: Imaginary parts of the field with $(x_p, y_p, z_p) = (0, 0, 100\,\mu\text{m})$. Cyan means 0 intensity

(real or imaginary part does not matter since we only want to know if the phase is sampled correctly) of the complex electrical field. In Figure 4.1a we can see the imaginary part of the electrical field U_0 at the front focal plane. The side length of the field is chosen to 500 µm inside the 4f-system code. We can see aliasing effects of high frequencies everywhere except the middle spot. Figure 4.1b shows the corresponding field ${U_1}^-$ after the FFT. Since the input is not sampled properly the results look at first not usable due to the artifacts. Luckily we only use the central spot of 10 000 µm diameter because our aperture is placed at the back focal plane. This cut out is shown in Figure 4.2a and we can observe that this spot is free of aliasing effects and contains all relevant information. Furthermore we can see the pattern is not circular symmetric anymore which is due to the cubic PM. One could also use smaller or larger input side lengths but chosen too large the sampling is not good enough anymore. Chosen too small it leads to artifacts as well because the decay of the input point source must be included to get correct results. In Figure 4.2b we can see an example where the side length is 50 µm and the

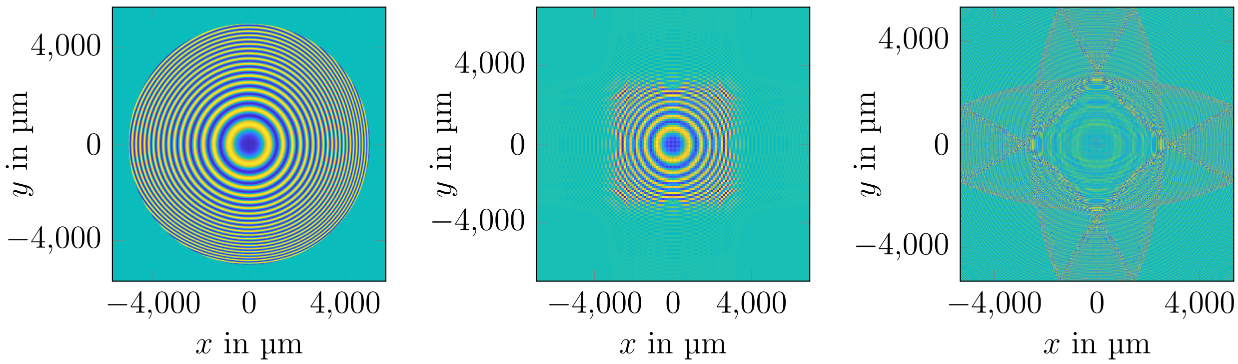

(a) LU0=500 µm (b) LU0=50 µm (c) LU=2000 µm

Figure 4.2: Imaginary part of U_1^+

input does not contain all information of the point source. On the other side in Figure 4.2c LU0 is too large and aliasing effects are present.

5 Simulation Results

In the last chapter we show how the PSFs of the LFM calculated by the three approaches look like. Furthermore we compare the resolution of setups with different positions of the PMs.

5.1 Point Spread Function

In this section we want to show the PSF of the 4f-system and how the PM placed at the Fourier plane influences the results. Furthermore we compare the different approaches derived in the previous sections.

4f-system without PM

First the 4f-system without the PM in the Fourier plane will be considered which is the situation in [Bro+13].

Theory from Cohen

In Figure 5.1 the simulated PSF of the 4f-system calculated with Equation 3.8 can be seen.

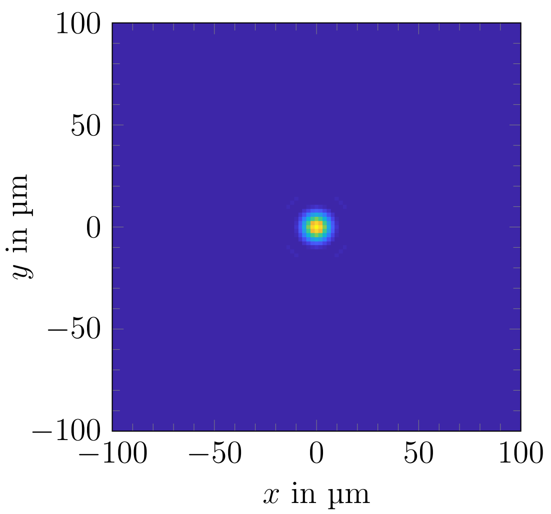

(a) Source position is (0 µm, 0 µm, 0 µm)

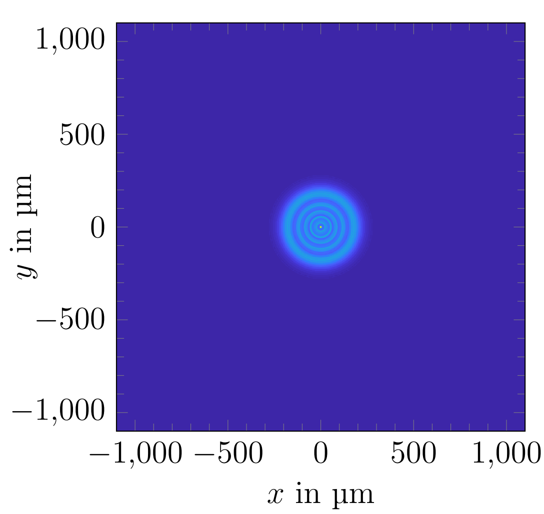

(b) Source position is (0 µm, 0 µm, 30 µm)

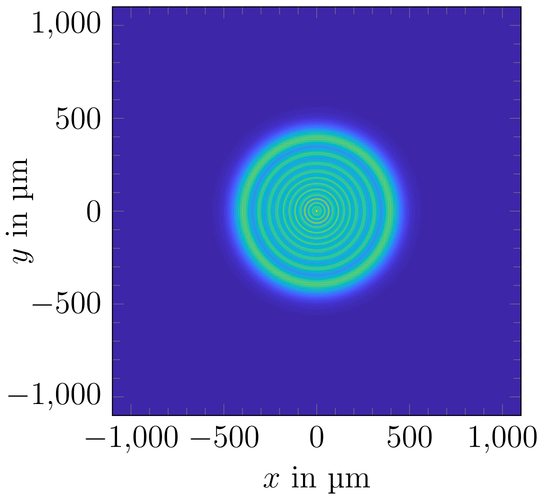

(c) Source position is (0 µm, 0 µm, 60 µm)

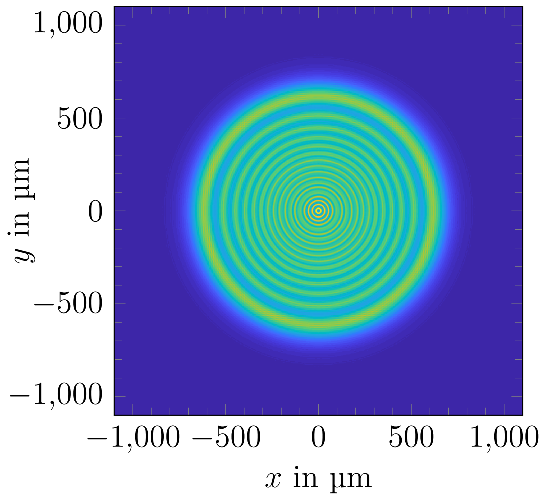

(d) Source position is (0 µm, 0 µm, 90 µm)

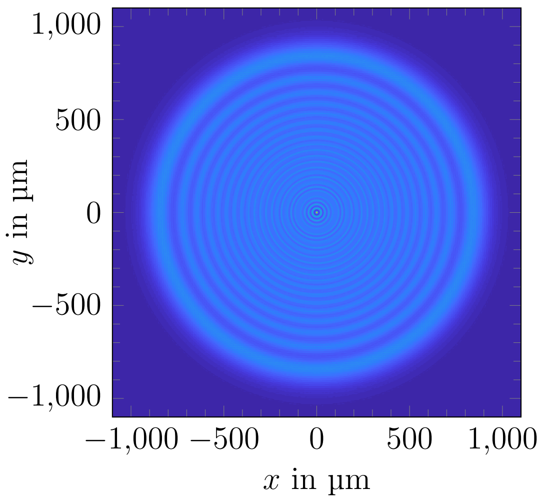

(e) Source position is (0 µm, 0 µm, 120 µm)

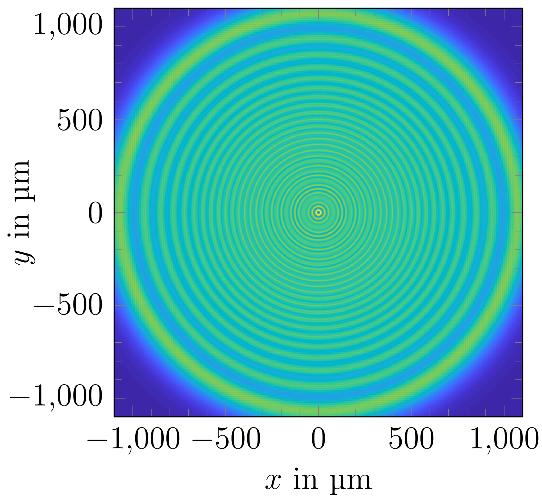

(f) Source position is (0 µm, 0 µm, 150 µm)

Figure 5.1: PSF of the 4f-system without PM

We only display the z_p from 0 µm to 150 µm. Negative z_p are exactly the same since the defocus is equal in both directions (with no aberrations). The PSF is furthermore shift invariant [Bro+13] and x_p, y_p can be set to 0 without loss of generality. The characteristic disk is sometimes called defocused Airy disk. The original Airy pattern is shown in Figure 5.1a but due to the intensity we only see the central spot and its diffraction limited size. Remember that a perfect and diffraction free system would only have one single point in the center instead of an extended spot.

Comparison

In Figure 5.2 we show the PSF for a depth equal to 60 µm. Between the Debye integral from [Bro+13] and the exact FFT approach from [Coh+15] we do not see any significant difference. We checked that for several relevant depths and it is quite reasonable. For a small NA one can show that the Debye integral is equal to the FFT relationship [Gu00]. However the third approach given by Equation 3.13 is not exactly equivalent to the previous one. We can observe a smaller extent of the spot in Figure 5.2f. This is peculiar since the FFT approach is a special case of the equation.

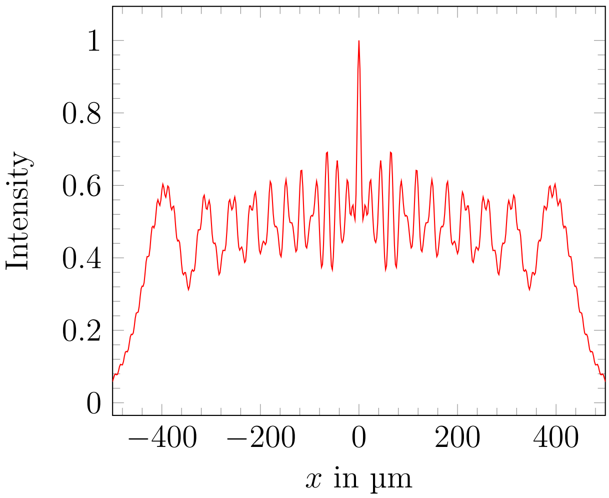

(a) Cross section PSF with Debye integral

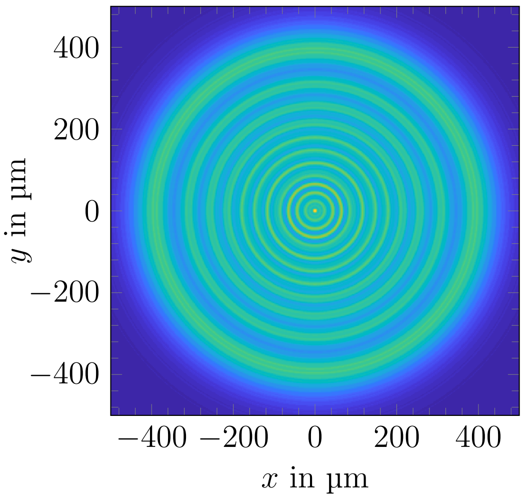

(b) PSF with Debye integral

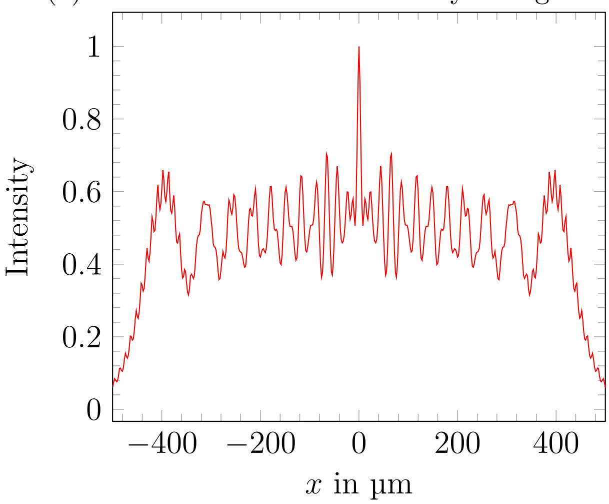

(c) Cross section PSF with exact FFT

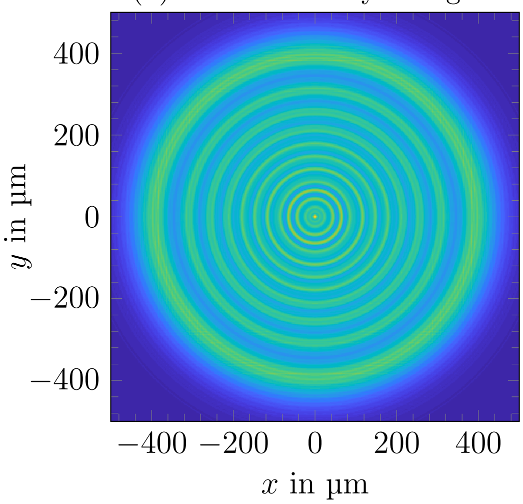

(d) PSF with exact FFT

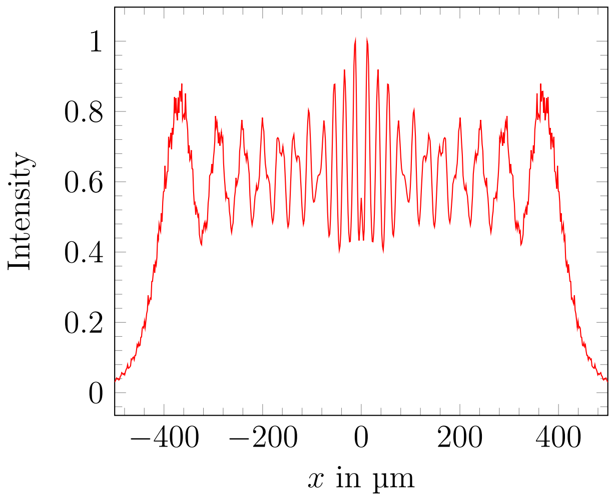

(e) Cross section PSF with Equation 3.13

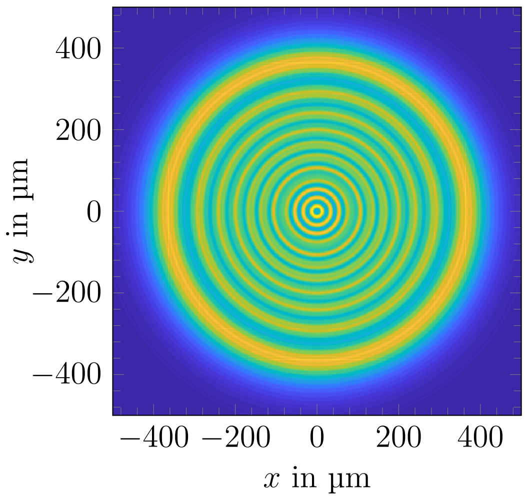

(f) PSF with Equation 3.13

Figure 5.2: PSF calculated with different equations and point source placed at $z_p = 60\,\mu\text{m}$

For the FFT approach we do an exact propagation of the spherical wave until the Fourier plane. From that we are using the FFT property from front focal plane to back focal plane. In Equation 3.13 we leave out this propagation and use the equation directly. The only explanation for the difference is the Fresnel approximation which is not that accurate for the NA = 0.5. For lower NA we checked that both approaches are converging to the same distribution. Our conclusion of this mismatch is that Fresnel is an approximation and the difference must result out of this. In Figure 5.3 and Figure 5.4 we visualized that for all depths the FFT approach is very similar to the Debye integrals.

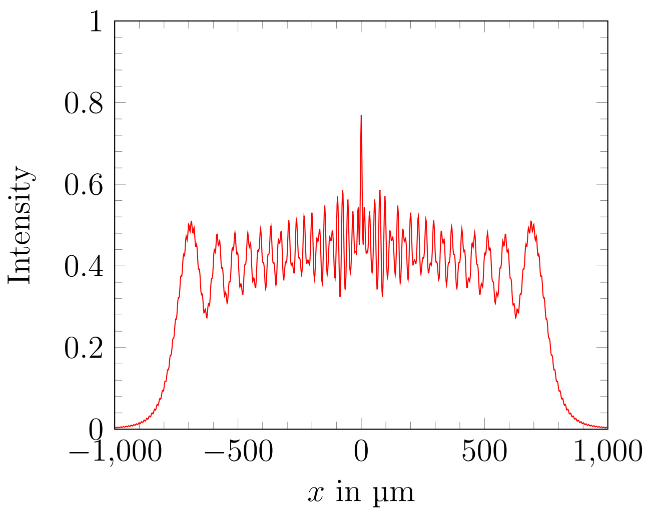

(a) Cross section PSF with Debye integral

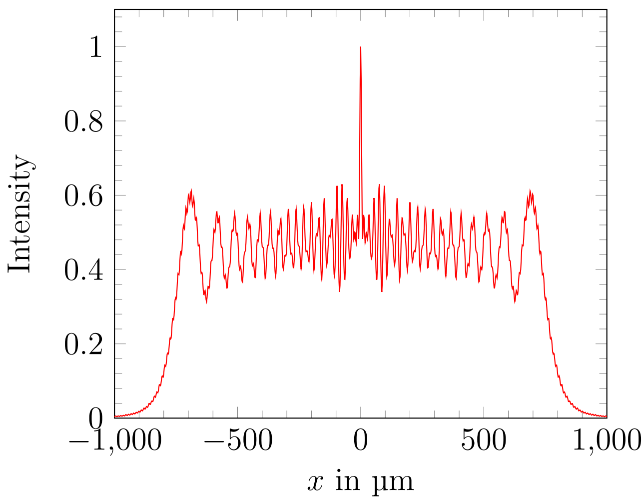

(b) Cross section PSF with FFT

Figure 5.3: PSF with $z_p = 100\,\mu\text{m}$

Although Debye includes aberrations and the FFT approach does not we can't see any big difference between both.

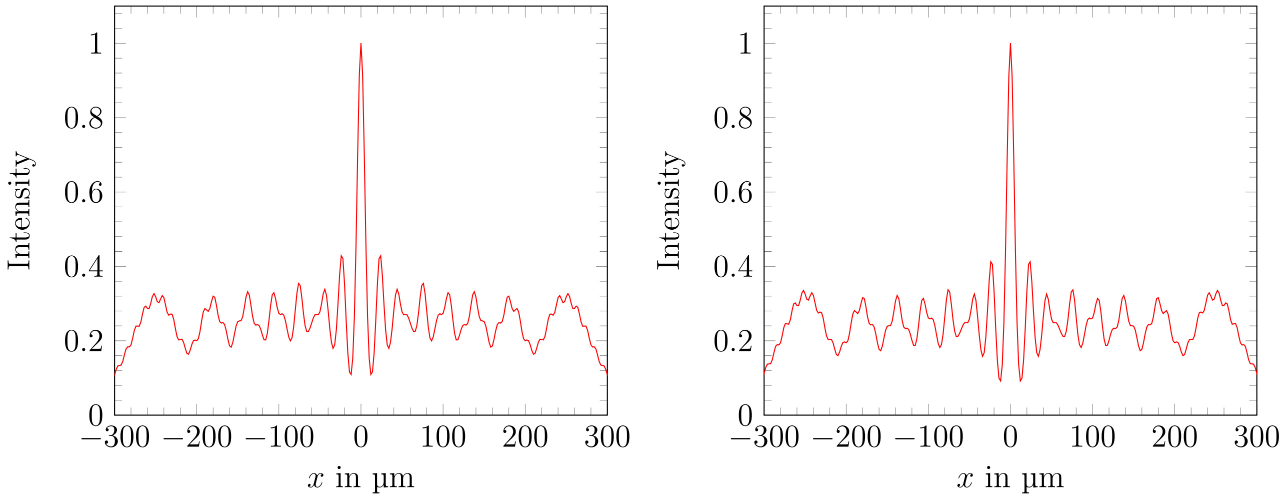

(a) Cross section PSF with Debye integral

(b) Cross section PSF with FFT

Figure 5.4: PSF with $z_p = 10\,\mu m$

Shift Invariance

The shift invariance for the 4f-system without PM was already mentioned in [Bro+13]. Fortunately, the PM does not break the shift invariance and we can still use this property for efficient reconstruction algorithms. From a physical point of view this is reasonable since placing the

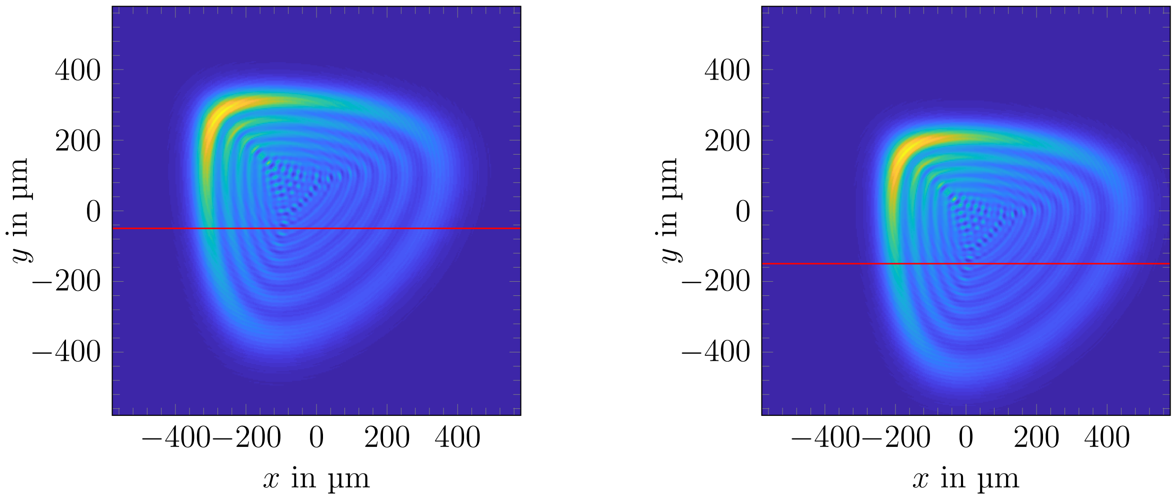

(a) $(50\,\mu m, 5\,\mu m, 5\,\mu m)$

(b) $(50\,\mu m, 0\,\mu m, 0\,\mu m)$

Figure 5.5: Shift invariance of the PSF

source position at $(x_p, y_p, z_p) \neq (0, 0, 0)$ changes the angle of the constant phase relative to the lens axis but the phase shift of the PM depends only on the position. An example of the shift is drawn in Figure 5.5. Additionally we did a cross section through the PSF (red line) in Figure 5.5 and plotted the values in Figure 5.6a both for the normal PSF and the shifted one. To verify that both are equivalent we overlayed and subtracted them from each other in Figure 5.6b. We can see that the difference is around 1/1000 of the absolute value. These differences arise out of numerical issues in the FFT and the downsampling at different position but in practice they are not relevant.

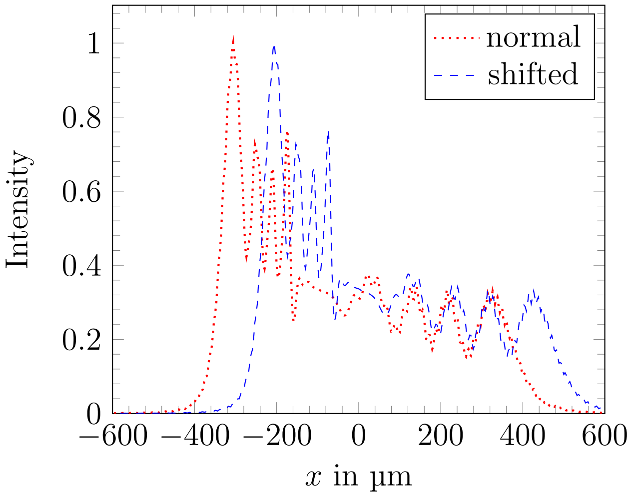

(a) Cross section PSFs

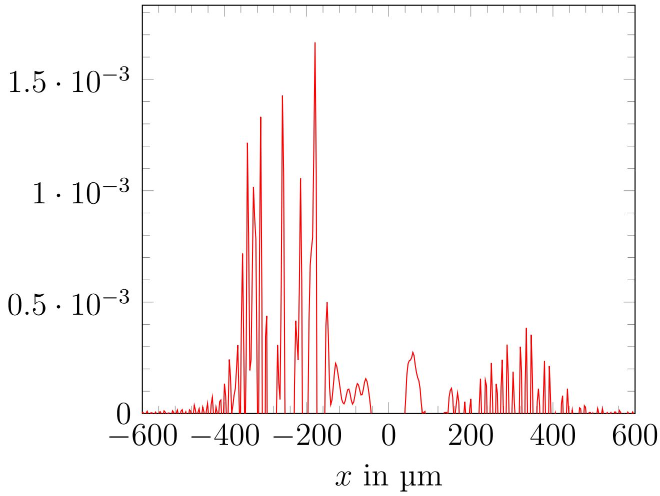

(b) Difference shifted and normal PSF

4f-system with PM

In this part we show some PSF results with the objective PM placed at the Fourier plane. The PM is defined by $\phi(x, y) = 117 \cdot (x^3 + y^3)$. 117 is the optimal value calculated by Fisher information in [Coh+15]. In Figure 5.7 we observe that the PSF is not circular symmetric as before what is caused by the PM which shifts the wave in a cubic manner. Especially in Figure 5.7a the shape is changed drastically in comparison to higher depths where it looks like the egg shaped form of the previous PSF. One drawback of the old design in [Bro+13] was that the PSF at the native image plane only spreads over one microlens which reduces the spatial resolution. This is tackled by the PM because on the native image plane the shape already has a high expansion.

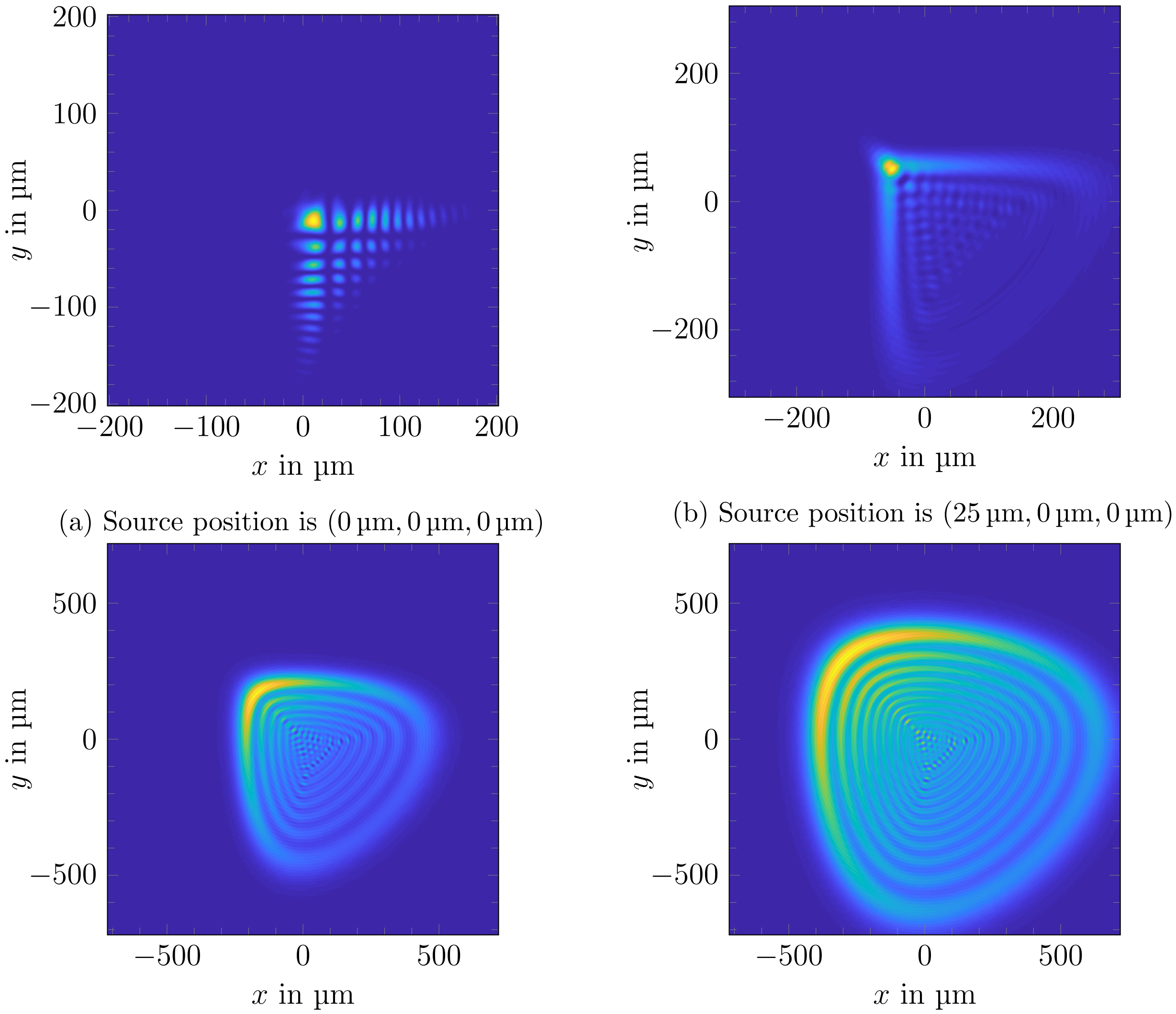

(a) Source position is (0 µm, 0 µm, 0 µm)

(b) Source position is (25 µm, 0 µm, 0 µm)

(c) Source position is (50 µm, 0 µm, 0 µm)

(d) Source position is (75 µm, 0 µm, 0 µm)

Figure 5.7: PSF of the 4f-system

PSF on sensor

Now we want to give a qualitative explanation why the resolution is higher using PMs as observed in [Coh+15]. In Figure 5.8a we show the PSF formed by the whole system at the native image plane without any PM. We see that only one microlens is affected. If we now shift the point source by 2 µm (see Figure 5.8b) we observe nearly the same pattern except the different substructure and some small strokes on 3 surrounding lenslets in the bottom right corner. This means that our system cannot distinguish between point sources shifted by a few micrometers very well.

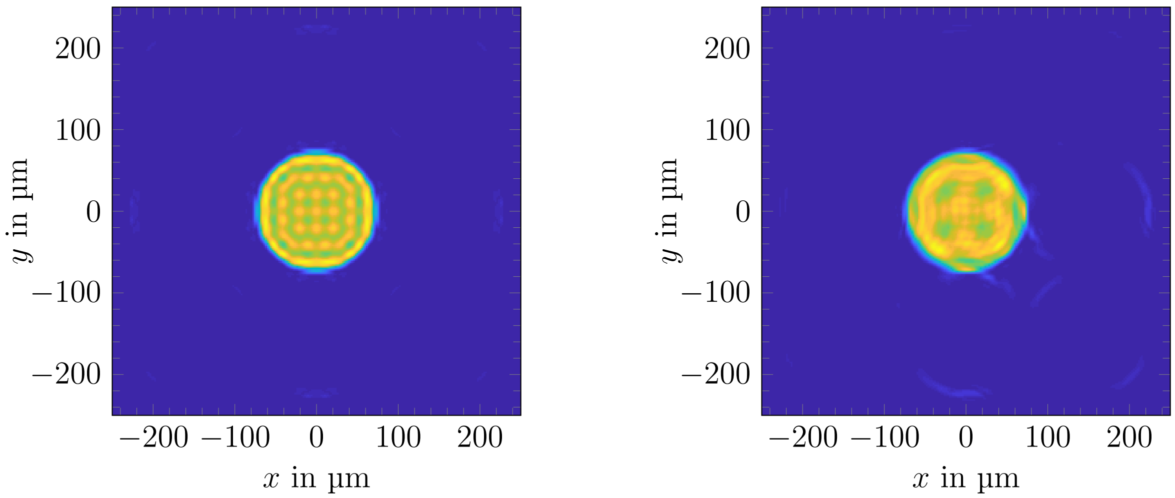

(a) Source position is (0 µm, 0 µm, 0 µm) (b) Source position is (0 µm, 2 µm, 2 µm)

Figure 5.8: PSF of the microscope with no PM

The situation changes a lot if we now place a PM at the Fourier plane of our system. The point source at the front focal plane creates a pattern which is spread over four microlenses and has a more characteristic substructure. Shifting the point source by a few micrometers in different directions alters the pattern more distinctly and is present on four microlenses in Figure 5.9d. This spreading is the key of the resolution enhancement of the native image plane because the point source is supported by more microlenses and the backprojection can be improved.

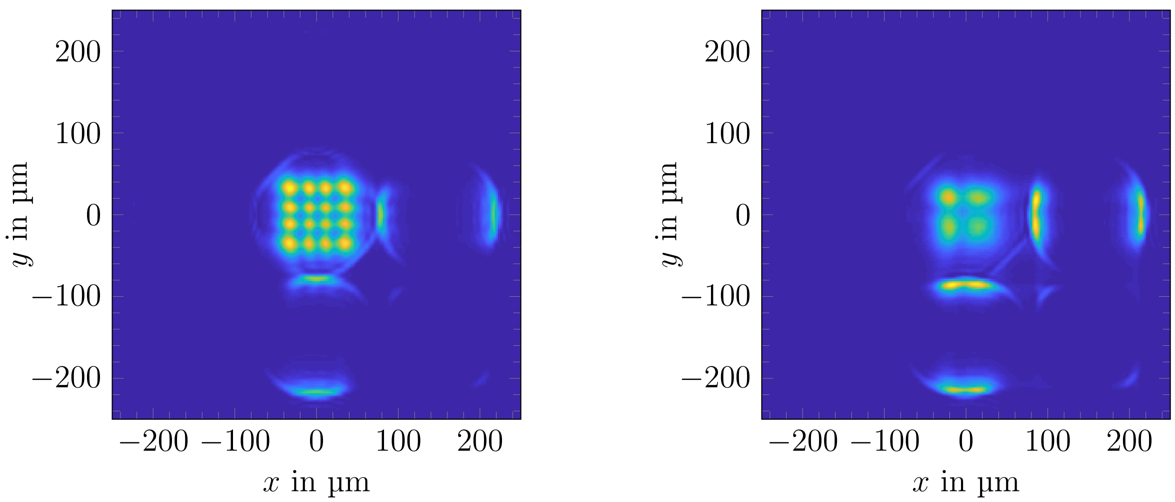

(a) Source position is (0 µm, 0 µm, 0 µm) (b) Source position is (0 µm, 1 µm, 1 µm)

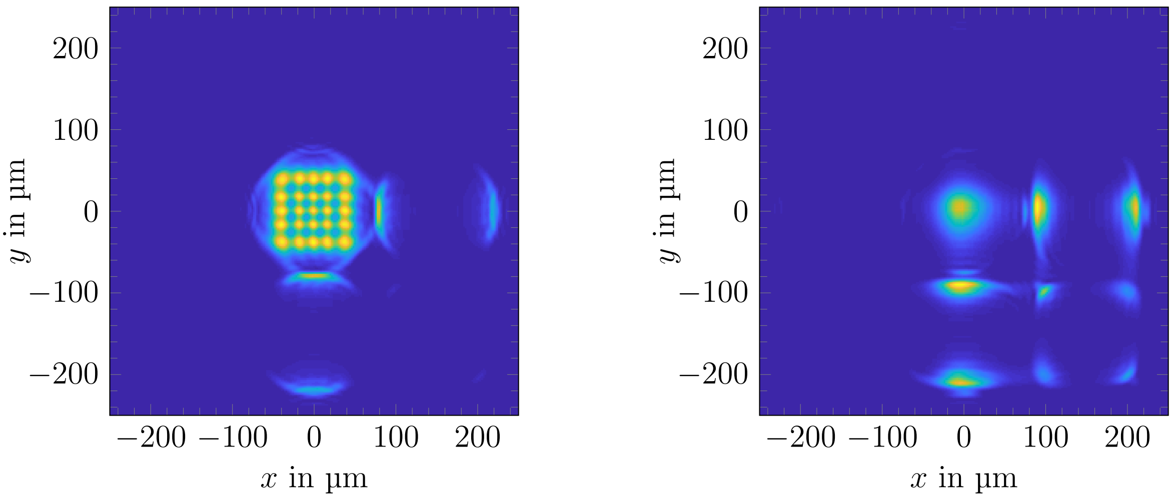

(c) Source position is $(0\,\mu\text{m}, -1\,\mu\text{m}, -1\,\mu\text{m})$ (d) Source position is $(0\,\mu\text{m}, 2\,\mu\text{m}, 2\,\mu\text{m})$

Figure 5.9: PSF of the microscope with objective, but no microlens PM

As a last improvement we can put a PM inside the MLA arrays. This PM is described by the function $\phi(x, y) = 5 \cdot (x^3 + y^3)$ and the input is normalized to the real physical size of the MLA so that $x, y \in [-1, 1]$. In Figure 5.10 we see an even more characterstic and individual pattern of the PSF. At the end we can say that the PSF of the 4f-system is simple optics and one was able

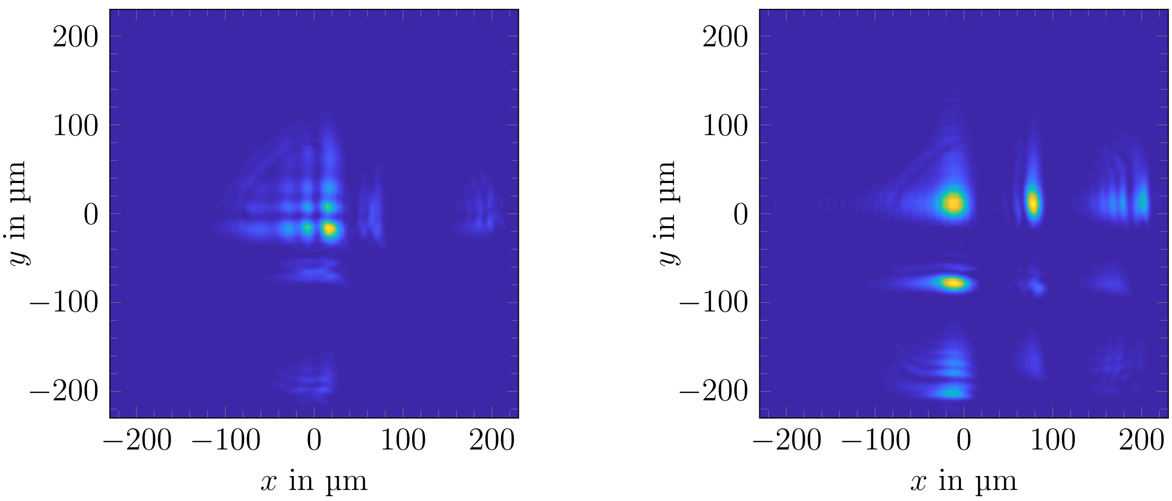

(a) Source position is $(0\,\mu\text{m}, 0\,\mu\text{m}, 0\,\mu\text{m})$ (b) Source position is $(0\,\mu\text{m}, 2\,\mu\text{m}, 2\,\mu\text{m})$

Figure 5.10: PSF of the microscope with objective and microlens PM

to understand the resulting pattern . But inserting the PMs and the MLA leads to a complete loss of the intuitive understanding of the system and the result has nothing much to do with conventional optics of a microscope.

5.2 Reconstruction Results

In the last part we want to show some reconstruction pictures of the simple target in Figure 5.11. The size of the boxes from top to bottom is 8.1 µm, 6.2 µm, 3.3 µm and 1.6 µm.

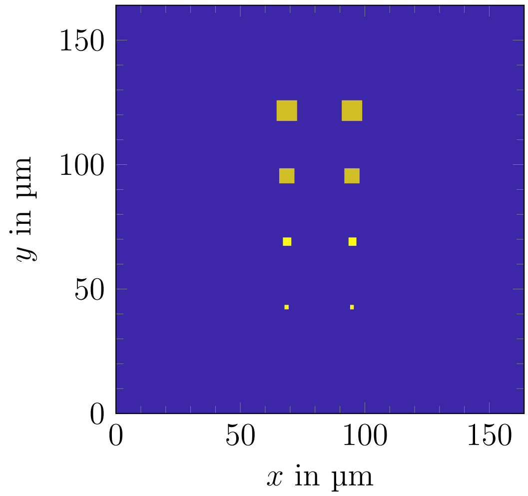

Figure 5.11: Test target

To generate the data to reconstruct we did a forward projection of the target with the calculated PSF. In Figure 5.12 the reconstruction results of the target after 75 iterations of the deconvolution algorithm are presented. Without any PM it is hard to recognize the smallest square in the bottom of the picture but for any other reconstruction where a PM was involved the square looks clearer to us. This is the resolution improvement mentioned in the previous sections.

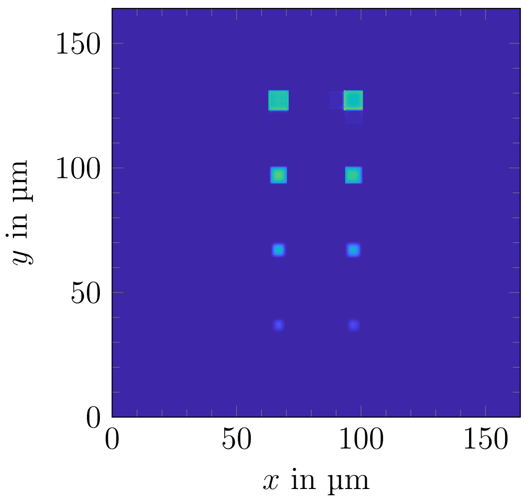

(a) No PM

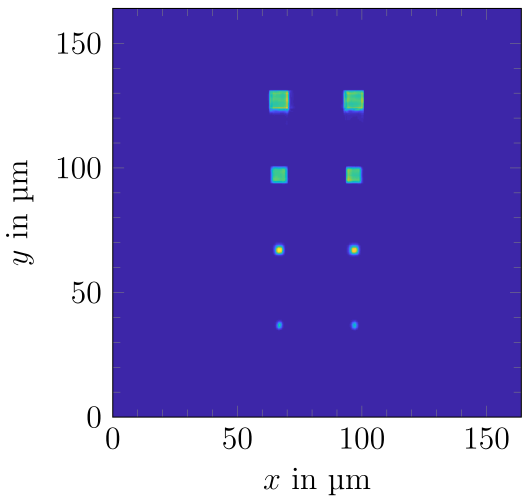

(b) objective PM

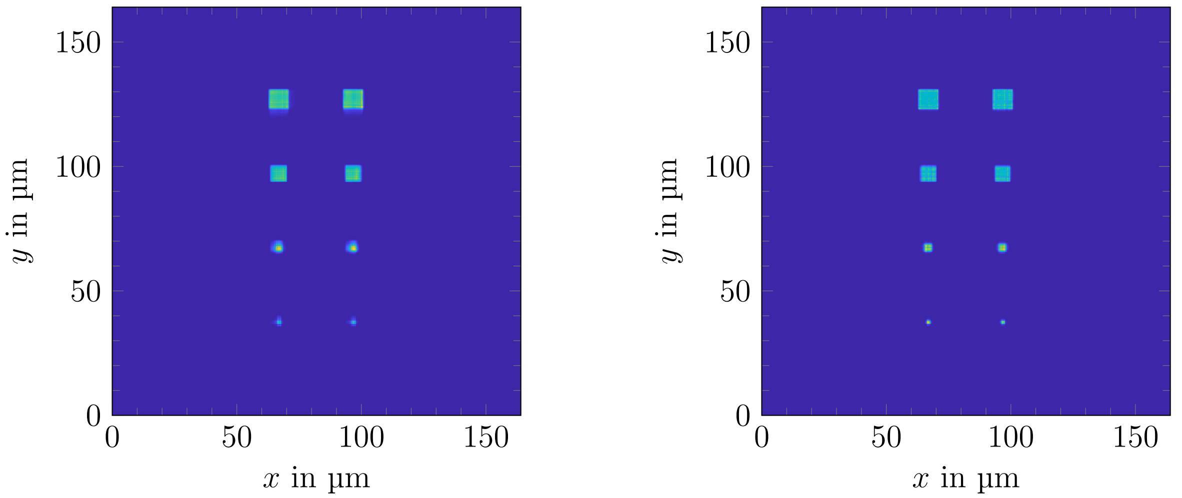

(c) MLA PM

(d) objective PM and MLA PM

Figure 5.12: Reconstruction of the native image plane

In Figure 5.13 we zoomed into the small squares. We can see that the intensity varies a lot within one square for the setup without PMs or only an objective PM. This means that we have blurred borders and low resolution. If we enable both PMs the variation is removed and also the borders look clearer, especially on the small squares.

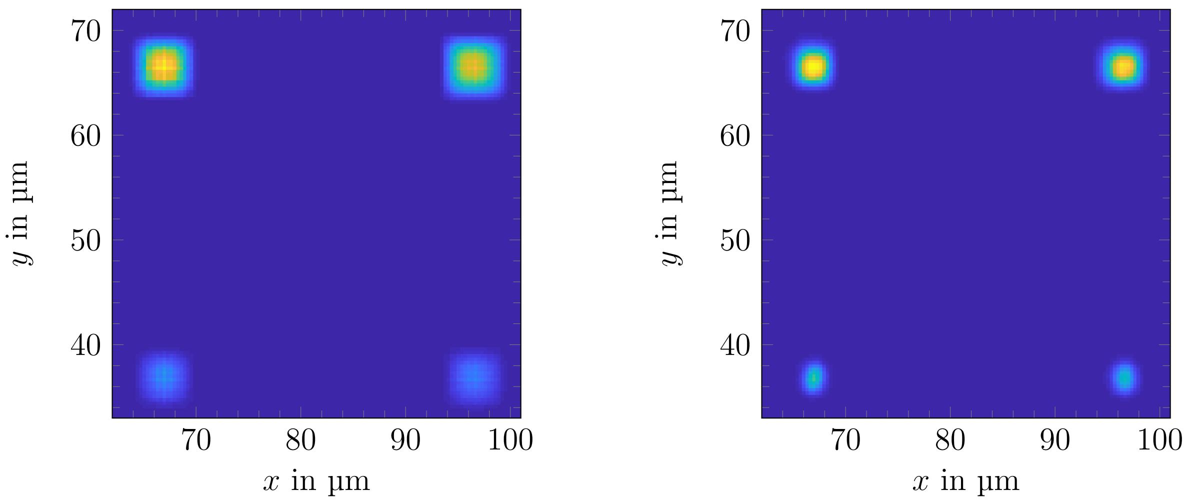

(a) No PM

(b) objective PM

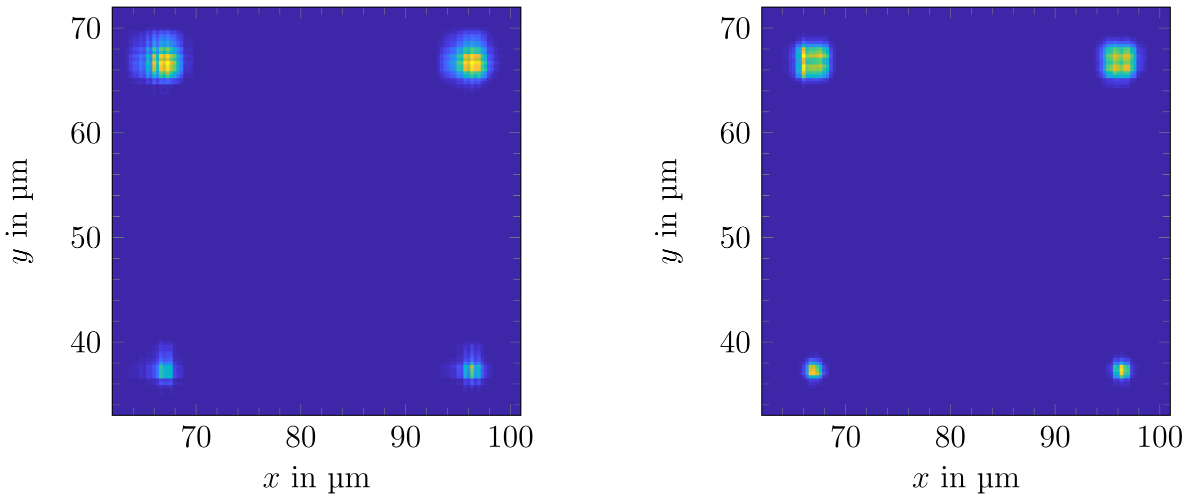

(c) MLA PM

(d) objective PM and MLA PM

Figure 5.13: Reconstruction zoomed in to bottom squares

Quantitatively the resolution of the image can be measured by the Modulation Transfer Function. Details about the calculation are given in [Coh+15]. In Figure 5.14 the resolution plots of our reconstruction can be seen. On the y-axis the resolution is given in line-pairs per mm. The color indicates the contrast of that resolution and yellow means that the resolution is well achieved. On the x-axis the different depths are shown. The PMs improve the resolution at the native plane a lot. For negative depths the resolution is a little bit worse than with PMs but the difference is negligible small. For positive depths the PM setup performs better.

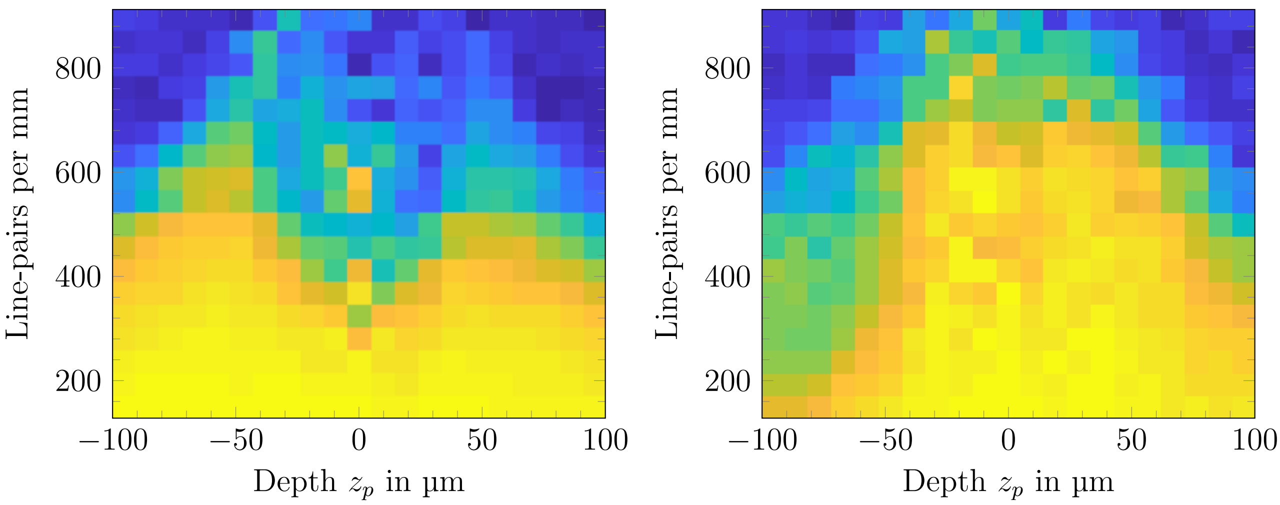

(a) Without PMs

(b) With objective and MLA PM

Figure 5.14: Resolution

6 Conclusion

In this thesis we derived the PSF of the LFM given in [Bro+13] starting at the basic of wave and Fourier optics. Based on this concepts we considered three different approaches for calculating the PSF and compared them to each other. We ascertained that Equation 3.13 does not coincide with the Debye integral and FFT approach in [Coh+15] for the given setup. The reason for this is the Fresnel approximation which can be inaccurate for high numerical apertures. We included the PMs into the system and justified that this increases the resolution and does not destroy the useful shift invariance. The optimal PMs were already found in [Coh+15] and we therefore concentrated on that one.
Possible research directions are systems with multiple focal lengths in the MLA. Including different PMs in each of the lenslets could increase the resolution further especially on the native plane. So far experiments were only done on systems with a PM placed at the Fourier plane. Setups with PMs placed inside or in front of the MLA are still an open task. Including aberrations in the 4f-system should not be that relevant as we saw in the comparison of the PSFs. However the incoming angles of the wave at the MLA can be very high which could lead to aberrations. These aberrations in the MLA are not modelled. At the moment we are using the initial light field camera setup called Plenoptic 1.0 but it was already shown in [GL09] that the new setup (Plenoptic 2.0) provides increased spatial resolutions. It would be interesting to test this setup in the use case of LFM.

Bibliography

[AW92] E. H. Adelson and J. Y. A. Wang. “Single lens stereo with a plenoptic camera”. In: *IEEE Transactions on Pattern Analysis and Machine Intelligence* 14.2 (Feb. 1992), pp. 99–106. ISSN: 0162-8828. DOI: 10.1109/34.121783.

[Bro+13] M. Broxton, L. Grosenick, S. Yang, N. Cohen, A. Andalman, K. Deisseroth, and M. Levoy. “Wave optics theory and 3-D deconvolution for the light field microscope”. In: *Opt. Express* 21.21 (2013), pp. 25418–25439. DOI: 10.1364/OE.21.025418.

[Chr12] L. W. Christian Perwaß. *Single lens 3D-camera with extended depth-of-field*. 2012. DOI: 10.1117/12.909882.

[Coh+14] N. Cohen, S. Yang, A. Andalman, M. Broxton, L. Grosenick, K. Deisseroth, M. Horowitz, and M. Levoy. “Enhancing the performance of the light field microscope using wavefront coding”. In: *Opt. Express* 22.20 (2014), pp. 24817–24839. DOI: 10.1364/OE.22.024817.

[Coh+15] N. Cohen, M. Levoy, R. Dror, and M. Horowitz. “A Wavefront Coded Light Field Microscope”. PhD thesis. Stanford University, 2015.

[FJ05] M. Frigo and S. Johnson. “The Design and Implementation of FFTW3”. In: *Proceedings of the IEEE* 93.2 (2005). Special issue on “Program Generation, Optimization, and Platform Adaptation”, pp. 216–231.

[Fre19] A. Fresnel. *Mémoire sur la diffraction de la lumière*. De l’Imprimerie de Feugueray, rue du Cloitre Saint-Benoit, no. 4, 1819.

[GL09] T. Georgiev and A. Lumsdaine. “Resolution in Plenoptic Cameras”. In: *Frontiers in Optics 2009/Laser Science XXV/Fall 2009 OSA Optics & Photonics Technical Digest*. Optical Society of America, 2009, CTuB3. DOI: 10.1364/COSI.2009.CTuB3.

[GLC11] T. G. Georgiev, A. Lumsdaine, and G. Chunev. “Using Focused Plenoptic Cameras for Rich Image Capture”. In: *IEEE Computer Graphics and Applications* 31.1 (2011), pp. 62–73. DOI: 10.1109/MCG.2011.12.

[Goo96] J. Goodman. *Introduction to Fourier Optics*. McGraw-Hill Series in Electrical and Computer Engineering: Communications and Signal Processing. McGraw-Hill, 1996. ISBN: 9780070242548.

[Gu00] M. Gu. *Advanced Optical Imaging Theory*. Springer Series in Optical Sciences. Springer, 2000. ISBN: 9783540662624.

[Huy90] C. Huygens. *Traité de la lumière: Ou sont expliquées les causes de ce qui luy arrive dans la reflexion, et dans la refraction Et particulierement dans l'etrange refraction du cristal d'Islande ; Avec un discours de la cause de la pesanteur*. Pierre Vander Aa, 1690.

[Lev+06] M. Levoy, R. Ng, A. Adams, M. Footer, and M. Horowitz. "Light Field Microscopy". In: *ACM Trans. Graph.* 25.3 (July 2006), pp. 924–934. ISSN: 0730-0301. DOI: `10.1145/1141911.1141976`.

[LH96] M. Levoy and P. Hanrahan. "Light Field Rendering". In: *Proceedings of the 23rd Annual Conference on Computer Graphics and Interactive Techniques, SIGGRAPH 1996, New Orleans, LA, USA, August 4-9, 1996*. 1996, pp. 31–42. DOI: `10.1145/237170.237199`.

[Ng+05] R. Ng, M. Levoy, M. Brédif, G. Duval, M. Horowitz, and P. Hanrahan. *Light Field Photography with a Hand-Held Plenoptic Camera*. Tech. rep. Apr. 2005.

[Smi+93] B. W. Smith, D. G. Flagello, J. R. Summa, and L. F. Fuller. "Comparison of scalar and vector diffraction modeling for deep-UV lithography". In: *Proc.SPIE* 1927 (1993), pp. 1927–1938. DOI: `10.1117/12.150481`.

[Som54] A. Sommerfeld. *Optics, volume IV of Lectures on Theoretical Physics*. Academic Press, Inc., New York, 1954.

[Voe11] D. G. Voelz. *Computational fourier optics: A MATLAB tutorial*. Bellingham, Wash: SPIE Press, 2011.

[WM64] E. Wolf and E. W. Marchand. "Comparison of the Kirchhoff and the Rayleigh–Sommerfeld Theories of Diffraction at an Aperture". In: *J. Opt. Soc. Am.* 54.5 (May 1964), pp. 587–594. DOI: `10.1364/JOSA.54.000587`.